

Eclipse Timings of the Transient Low Mass X-ray Binary EXO 0748–676. IV. The Rossi X-Ray Timing Explorer Eclipses

Michael T. Wolff¹, Paul S. Ray², Kent S. Wood³

Space Science Division, Naval Research Laboratory, Washington, DC 20375-5352

and

Paul L. Hertz⁴

Science Mission Directorate, NASA Headquarters, Washington, DC 20546-0001

ABSTRACT

We report our complete database of X-ray eclipse timings of the low mass X-ray binary EXO 0748–676 observed by the *Rossi X-Ray Timing Explorer* (*RXTE*) satellite. As of this writing we have accumulated 443 full X-ray eclipses, 392 of which have been observed with the Proportional Counter Array on *RXTE*. These include both observations where an eclipse was specifically targeted and those eclipses found in the *RXTE* data archive. Eclipse cycle count has been maintained since the discovery of the EXO 0748–676 system in February 1985. We describe our observing and analysis techniques for each eclipse and describe improvements we have made since the last compilation by Wolff et al. The principal result of this paper is the database containing the timing results from a seven-parameter fit to the X-ray light curve for each observed eclipse along with the associated errors in the fitted parameters. Based on the standard O – C analysis, EXO 0748–676 has undergone four distinct orbital period epochs since its discovery. In addition, EXO 0748–676 shows small-scale events in the O – C curve that are likely due to short-lived changes in the secondary star.

Subject headings: X-rays: binaries, binaries: eclipsing, stars: individual (EXO 0748–676)

¹E-mail Address: Michael.Wolff@nrl.navy.mil

²E-mail Address: Paul.Ray@nrl.navy.mil

³E-mail Address: Kent.Wood@nrl.navy.mil

⁴E-mail Address: Paul.Hertz@nasa.gov

1. Introduction

The orbital period is one of the most fundamental parameters characterizing binary star systems. Understanding the evolution of binary systems requires understanding how the orbital period might change on both short and long time scales, both from a theoretical and observational standpoint. As a binary system evolves mass and angular momentum are exchanged between the binary components, angular momentum is carried out of the system via mass loss, and each component can evolve via either nuclear compositional and stellar structural changes. Eclipse transitions provide good fiducial timing markers allowing the precise timing of the orbit which, in turn, make possible the long-term characterization of period changes and the magnitude of the effects these physical processes have on the system parameters.

To date, five low mass X-ray binaries (LMXBs) showing full X-ray eclipses are known (EXO 0748–676, X1658–298, XTE J1710–281, AX J1745.6–2901, and GRS J1747–312). Of these sources, only EXO 0748–676 has been persistently X-ray active over the past two decades and thus available for continuous monitoring of its orbital period behavior (Parmar et al. 1986; Wolff et al. 2002). EXO 0748–676 is a transient X-ray system with a 3.82 hour orbit period first observed by the European Space Agency’s X-ray Observatory (*EXOSAT*) satellite when it became X-ray active in February of 1985 (Parmar et al. 1986). It has remained X-ray active at a level of at least a few mcrab since its discovery. The eclipsing LMXB X1658–298 was discovered by the SAS-3 satellite in October 1976 (Lewin et al. 1976) and was eventually determined to be a X-ray bursting, eclipsing LMXB with an orbital period of 7.12 hours (Cominsky & Wood 1989). X1658–298 became undetectable in X-rays in 1979 but then returned to X-ray activity in April 1999, repeatedly being observed by BeppoSAX (Oosterbroek et al. 2001) and the *Rossi X-Ray Timing Explorer (RXTE)* (Wachter et al. 2000) until it became X-ray inactive again in October 2000. The observations reported by Wachter et al. (2000) appeared to indicate that the orbital period was changing with a time scale of $\tau_{orb} = |P_{orb}/\dot{P}_{orb}| \sim 10^7$ years even though little mass transfer had occurred between epochs of X-ray activity. X1658–298 has remained X-ray inactive since October 2000 making long term monitoring of its X-ray orbital period impossible.

GRS J1747–312 in globular cluster Terzan 6, and XTEJ1710–281 are both regularly recurring transient sources showing full X-ray eclipses and have orbital periods 12.4 hours and 3.28 hours, respectively. Their ephemerides can be established via X-ray observations (in’t Zand et al. 2003). However, in the case of GRS J1747–312, timing observations based on the mid-eclipse timings are difficult because of the relatively long eclipse totality (~ 43 minutes). Eclipse observations must wait through a long duration of totality when virtually no X-ray activity from the source can be seen in order to accurately time both the ingress and

egress transitions of any single eclipse. Finally, the transient faint source AX J1745.6–2901 is very close to Sgr A* and thus very difficult to observe because of source confusion in that crowded field. Nevertheless, it has been detected by both the Advanced Satellite for Cosmology and Astrophysics (*ASCA*) (Maeda et al. 1996; Sakano et al. 2002) and by the X-ray Multi-Mirror Mission (*XMM-Newton*) with the 23-minute eclipse variations being visible and the orbital period measured at 8.36 hours (Porquet et al. 2007).

For all of these reasons, EXO 0748–676 is a uniquely good system for long-term study of LMXB orbital evolution. Thus, early in the *RXTE* mission, we began a program of monitoring the X-ray eclipses in EXO 0748–676 in an effort to detect orbital period variations. The ultimate goal at that time was to measure the orbital period derivative \dot{P}_{orb} and compare this with estimates of magnitude of orbital period changes in theoretical calculations of LMXB evolution. EXO 0748–676 was observed intensely by the EXOSAT satellite (Parmar et al. 1986) resulting in the first estimate of its orbital period and also revealing that, because the source showed X-ray bursts, the compact object in the binary was a neutron star. It should be noted, however, that even the 23-year time baseline reported on here is short compared to the time steps in most evolutionary calculations of binary systems which are in the range $\Delta t > 10^{4-5}$ years. Theoretical calculations of LMXB evolution must cover a time span of 1-10 Gyrs and time-steps less than 10^4 years would make such computations prohibitively expensive. Thus, we still have yet to access a sufficiently long baseline to allow robust comparison with most theoretical calculations of LMXB evolution. Conversely, most theoretical calculations do not resolve binary system effects, such as magnetic field generation and cycling in the secondary star, that can potentially influence the system O – C behavior on our 23-year observational time scale.

With these monitoring observations we expected to find smooth variations in the O – C residuals (observed minus calculated residuals are the delay or advance in the mid-eclipse timings compared to that expected for a specified ephemeris) that could be compared to the estimates of LMXB evolutionary time scales predicted by theory (e.g., Rappaport et al. 1982). What we found was considerably more complicated. The first paper in this series, Hertz et al. (1995), concluded that the variable eclipse durations and profiles observed in EXO 0748–676 implied there is an additional source of uncertainty in timing measurements and that this uncertainty is intrinsic to the binary system, correlated from observation to observation, and had variance that increased as a function of binary cycles between observations. Hertz et al. also suggested that spurious trends in the O – C residuals could be misinterpreted as changes in the orbital period. Hertz et al. (1997) went further and identified a component of “intrinsic scatter” in the O – C residuals of ~ 0.15 s per orbit cycle. Finally, Wolff et al. (2002) found that neither a constant orbital period derivative or any reasonable polynomial expansion in P_{orb} , \dot{P}_{orb} , etc., provided an acceptable fit to the entire

historical set of O – C residuals. Rather, the system appeared to go through “epochs” in which the orbital period would change on the order of milliseconds from epoch to epoch. A model for the observed O – C variations that included observational measurement error, cumulative orbital period jitter intrinsic to the binary system, with some underlying period evolution was found to be consistent with the observed mid-eclipse timing data and implied a rapid timescale for orbit evolution, $\tau_{orb} \sim 2 \times 10^7$ years.

2. Full Eclipse Observations

2.1. *RXTE* Observations

We utilize all observations from the *RXTE* satellite (Jahoda et al. 1996; Jahoda et al. 2006) of EXO 0748–676 from which we can isolate a full X-ray eclipse. We number the eclipses using the numbering scheme of Parmar et al. (1986) but with a revised ephemeris: $T_0(\text{TDB; MJD}) = 46111.0751315$ and $P_{orb} = 0.1593377866$ days. We reduced each observation data set with the HEASoft software version 6.5 released on June 26, 2008. We utilize the combined background model released on August 6, 2006 available at the *RXTE* web site¹. These software releases are corrected for the problems with the background estimation algorithms and the Proportional Counter Array (PCA) effective area calibration that makes the Crab flux come out at its standard value (see Jahoda et al. 2006).

The observations of EXO 0748–676 we analyze generally fall into two categories. First, there are our systematic monitoring observations or “campaigns”. These are tightly clustered observations over about one day of a series of eclipses, perhaps consecutive, made around the approximate predicted eclipse times, giving us a look at the pre-eclipse flux level for several hundred seconds, the full eclipse profile, and finally the post-eclipse flux level, again for several hundred seconds. The duration of X-ray eclipse in EXO 0748–676 is approximately 495 seconds (~ 8.3 minutes) and so a complete observation consists of as little as ~ 1.5 ks of PCA time. This makes EXO 0748–676 a good target for eclipse timing compared to, say, GRS1747–312, with its 43 minute totality duration. Virtually all of our monitoring eclipse observations, except those early in 1996, were made with the GoodXenon Experiment Data System (EDS) mode. Early 1996 observations, however, done before we had much experience with the PCA response to X-ray sources, were made with the E_62us_64M_0_1s, E_8us_32B_0_1s, E_125us_64M_0_1s, E_250us_128M_0_1s EDS modes. The second general

¹PCA X-ray background model information is found at the web site http://rxte.gsfc.nasa.gov/docs/xte/pca_news.html.

type of observation are those observations of EXO 0748–676 that were done for other scientific reasons such as to probe quasi-periodic oscillations or searching for X-ray bursts and are found in the High Energy Astrophysics Science Archive Research Center (HEASARC) public archive at Goddard Space Flight Center. Generally, these observations are done in an event mode such as E_125us_64M_0.1s.

Early in the *RXTE* mission our campaign observations, indeed most observations of any source, utilized the full complement of 5 Proportional Counter Units (PCUs). As the problems developed over time with various PCUs the number of PCUs in any one observation was reduced so that by the end of the *RXTE* mission it is not unheard of for only one or two PCUs to be turned on for a particular observation. In the case of GoodXenon data both layer and PCU information is preserved in the raw data files we start with and thus we can select events based on PCU and anode layer within each PCU. On the other hand, generally for the event modes, layer information (and sometimes PCU information) was not available in the raw data files.

During most observations the background count rates in one PCU for layer 1 in the energy range 2–20 keV are around 7–10 counts s^{−1} PCU^{−1}. If the observation mode is GoodXenon we select events occurring in layer 1 from those PCUs on during the entire eclipse observation thus keeping the background count rate low. On the other hand, if we must use events from all layers then typical background count rates in the same energy range will be significantly larger, increasing the Poisson errors and making the eclipse light curves more noisy. If a PCU turned on or off during an eclipse this would lead to variations in the background level and source count rates that invalidated our model for the simple ingress/egress fitted shape of the eclipse. Furthermore, when a PCU is turned on or off during an observation this can lead to count rate transients that interfere with our eclipse fitting. We screened our observations for such effects and when they were found we first tried to recover a fitable eclipse profile by excluding events from the PCU that was turned on/off during the observation. If for any reason it was not possible to exclude only the offending PCU then we excluded the entire eclipse. Finally, we note that we make no effort to exclude either of the PCUs that have no Propane layer but instead simply accept the events from those PCUs and utilize the existing background estimates from *pcabackest*.

We proceeded as follows for our analysis of each eclipse: We extracted light curves as described above for each eclipse, screening the observations for electron or other transient instrument events that can sometimes degrade PCA performance, and when such problems did occur and they affected the entire light curve we would exclude that eclipse from our analysis. In rare instances short data dropouts can occur during an observation that show up as either gaps in the final source light curve or as 2-second segments for which, regardless

of the true source plus background count rate, the count rate goes to zero. In general, we mask such regions out of the analysis by selecting events outside the relevant time intervals. However, we exclude the entire eclipse from analysis if such a corrupted region in the light curve affects a transition feature (ingress or egress) in the fitted light curves. In those cases where there was an X-ray burst either during totality or in the parts of the uneclipsed light curves we fit to, we masked out the part of the light curve containing visible signs of the burst in order not to bias the estimate of the normal X-ray count rate. The only exception to this was when a burst occurred sufficiently close to either the ingress or egress to distort the shape of the transition. In this case we excluded the eclipse from further analysis. The background was estimated with the FTOOL *pcabackest* utilizing the faint-source model, the resulting source+background and background light curves were barycentered with the FTOOL *faxbary*, and then the background was subtracted from the source+background light curve to produce a source-only barycentered lightcurve showing the full eclipse. The barycentering FTOOL *faxbary* has an absolute timing accuracy of better than $100\mu\text{s}$ which is sufficient for our purposes (see Rots et al. 1998). This resulting source-only light curve, usually binned at 0.5 s, was then fitted with our seven-parameter ramp-and-step model for the basic eclipse variations.

2.2. Eclipse Fitting and Error Estimates

Our model for a full X-ray eclipse consists of seven parameters: the pre-ingress (F_{in}), totality (F_{ec}), and post-egress (F_{eg}) count rates (uncorrected for number of PCUs), the durations of the ingress (Δt_{in}) and egress (Δt_{eg}), the duration of totality (Δt_{ec}) and finally the barycentered mid-eclipse time (t_{mid}). An alternative model for the eclipse times is the times of the four “contacts”: t_1 , t_2 , t_3 , and t_4 . The relationship between the two timing systems is simple:

$$t_1 = t_{mid} - \frac{1}{2}\Delta t_{ec} - \Delta t_{in}, \quad (1)$$

$$t_2 = t_{mid} - \frac{1}{2}\Delta t_{ec}, \quad (2)$$

$$t_3 = t_{mid} + \frac{1}{2}\Delta t_{ec}, \quad (3)$$

$$t_4 = t_{mid} + \frac{1}{2}\Delta t_{ec} + \Delta t_{eg}. \quad (4)$$

A fitted eclipse from an observation utilizing only one PCU is shown in Figure 1. The eclipse light curve fit results in the parameters with error estimates that are listed for each eclipse in Table 1, and constitutes the principal result of this paper. All of the errors quoted

in Table 1 come from this fitting process. We also show in the table the fit reduced χ^2 value (χ^2_ν) and the number of PCUs utilized during each observation. We compile a second table of those eclipses or partial eclipses observed by *RXTE* that we can not fit with our seven-parameter model in Table 2, each for the reason indicated.

The fitted mid-eclipse time in Table 1 is simply $t_{mid} = (t_2 + t_3)/2$, the half-way point between the end of ingress and the beginning of egress. When the ingress and egress profiles are relatively smooth and the count rate changes monotonically, even in those cases where the ingress or egress durations are relatively long, we find the mid-eclipse time can be determined with a typical accuracy of $\sim 1/2$ s. If, on the other hand, the ingress or egress changes are not monotonic, such as is the case with the momentarily reversing ingress profiles discussed in Wolff et al. (2007), then determining the mid-eclipse times becomes more difficult because the applicability of our seven-parameter eclipse model becomes problematic. In such a case a more sophisticated model for the eclipse variations must be employed and the errors must be determined in some new fashion that will depend on the model chosen. This is a point to which we return below.

During the fit process, in order to analyze the O – C behavior of the system carefully [e.g., as was done in Wolff et al. (2002)], we must make a robust estimate of the errors in the fitted mid-eclipse times. A careful analysis of the errors in all seven parameters in as analytically rigorous as possible would be very computationally complex and too costly in outlay of effort relative to the quality of the resulting error estimates. Thus, we employ a less formally rigorous but more computationally tractable procedure to estimate the errors in the fitted parameters listed in Table 1. First, we utilize a very careful algorithm to find the best fit eclipse model and global minimum χ^2 value in the seven-parameter fit space for our eclipse model. Once we have the best fit model parameters and χ^2_{min} we then carefully search in the mid-eclipse time parameter t_{mid} around this χ^2_{min} until we have those values of the mid-eclipse time both above and below t_{mid} for which χ^2 increases by 1 over χ^2_{min} . This gives us two time intervals, one above t_{mid} and one below t_{mid} , representing the error time interval for t_{mid} and it is the average of these two intervals that we give as the error in t_{mid} in Table 1 column 4. We employ a similar procedure to estimate the errors in the eclipse widths (Δt_{ec}) in Table 1. The results of this process are illustrated in Figure 2 for an example eclipse where the pre- and post-eclipse count rate is relatively low, in part because only one PCU was employed during the observation. However, in order to save computational complexity, we crudely estimate the errors in the other fit parameters based on the square root of the covariance matrix diagonal elements: $\sigma_{a_i} \sim \sqrt{cov(a_i, a_i)}$ where a_i is the parameter of interest and $cov(a_i, a_j)$ is represents the element of the fit covariance matrix for parameters a_i and a_j . Thus, we are implicitly assuming that the variation in χ^2 for the other five parameters in the fit are parabolic in the region around χ^2_{min} (e.g.,

Bevington & Robinson 2003).

3. Observed Ephemeris Behavior

Figure 3 shows the O – C diagram for the entire eclipse database from *EXOSAT*, the GINGA X-ray satellite, *ASCA*, the Roentgen Satellite (*ROSAT*), and the Unconventional Stellar Aspect experiment (*USA*). The sign convention for the O – C is such that O – C will be positive for an observed mid-eclipse time coming after the calculated (ephemeris predicted) time. No simple polynomial expansion in P_{orb} , \dot{P}_{orb} , \ddot{P}_{orb} , etc., can fit the O – C variations apparent in the figure. However, four epochs of general O – C behavior are evident from Figure 3. A piecewise linear function of mid-eclipse time representing the orbital period in the four distinct epochs can approximately represent the general trends in the O – C curve. In such a model we constrain the orbital phase to be constant across the instantaneous period change but allow the cycle of the change to be a free parameter. Such a function can be written in the form:

$$T_n = \begin{cases} T_0 + nP_{\text{orb},0} & \text{if } n \leq n_{b,0}, \\ T_0 + n_{b,0}P_{\text{orb},0} + (n - n_{b,0})P_{\text{orb},1} & \text{if } n_{b,0} < n \leq n_{b,1}, \\ T_0 + n_{b,0}P_{\text{orb},0} + (n_{b,1} - n_{b,0})P_{\text{orb},1} + (n - n_{b,1})P_{\text{orb},2} & \text{if } n_{b,1} < n \leq n_{b,2}, \\ T_0 + n_{b,0}P_{\text{orb},0} + (n_{b,1} - n_{b,0})P_{\text{orb},1} + (n_{b,2} - n_{b,1})P_{\text{orb},2} + (n - n_{b,2})P_{\text{orb},3} & \text{if } n_{b,2} < n. \end{cases} \quad (5)$$

where the eclipse cycle number is n , the $n_{b,i}$ are the cycle numbers where transitions from one period to another period are made, and the orbital periods in each epoch are $P_{\text{orb},i}$. Table 3 gives the results of such a piecewise fit to all the mid-eclipse times for EXO 0748–676. This solution for the orbital period is only an approximate representation of the O – C behavior on several year time scales and the formal χ^2 value for the fit is very poor. The individual O – C residuals are often clumped either above or below the solution line in the figure indicating that variation in the orbital period is occurring that our four-epoch solution does not capture. Thus, no formal errors are quoted in Table 3 for the parameters of the fit to equation 5. The systematic wandering of the mid-eclipse timings around the mean period noted by Hertz et al. (1997) and Wolff et al. (2002) has continued for all the eclipses observed by *RXTE*.

Based on our four-epoch solution to the O – C variations shown in Figure 3 it is apparent that at least four distinct orbital period epochs have occurred in the EXO 0748–676 system since its discovery in 1985. The three epochs that have occurred during the *RXTE* mission alone are shown in Figure 4 and this figure also includes seven eclipses observed by the *USA* experiment that operated from May 1999 to November 2000. One of these orbital period epochs is completely sampled by the *RXTE* observations, namely, the 4.8 years from MJD

51611 to MJD 53363.

Wolff et al. (2007) reported a consecutive series of eclipses where the occulting edge of the secondary star appeared to be modified from a simple hydrostatic atmosphere by a magnetically confined loop suspended above the secondary star’s surface. In their model the loop absorbed X-rays from the neutron star accretion disk just before ingress casting a X-ray shadow as seen at the earth and modifying the normal ingress transition profile. The five eclipses involved in that event are shown by the arrow at MJD 52978 in Figure 4. It is precisely for such eclipses, where the ingress or egress profiles consist of other than simple smooth, monotonically changing count rates, that our seven-parameter model for the eclipse profile breaks down and the fitted mid-eclipse time errors are no longer reliable. However, even in such cases our simple fits can yield the useful information of how such anomalous eclipses are bunched together over time, i.e., how much the system “remembers” the anomalous transitions from eclipse to eclipse (Koen 1996; Hertz et al. 1997; Wolff et al. 2002).

In their discussion of the magnetic eclipses, Wolff et al. (2007) stated that roughly 93 days after the first set of anomalous eclipses the eclipse profiles became particularly sharp and stable. The evidence supporting this claim can clearly be seen in Figure 5 where we plot the duration of eclipse (Δt_{ec}) as a function of time for the Table 1 eclipses. Analysis of the anomalous eclipses studied by Wolff et al. (2007) reveals large variations in the O – C residuals, due primarily to the long durations in the ingress times. However, eclipses in the range MJD = 53071 – 53229 have shorter durations (~ 490 seconds) and significantly smaller mid-eclipse time and eclipse duration uncertainties when compared to the eclipses on either side of this MJD range. During the eclipses analyzed by Wolff et al. the secondary was in a more extended state with the radius of its X-ray occulting edge at a larger value than the more stable eclipses coming ~ 93 days later.

Examination of Figure 3 strongly suggests that the EXO 0748–676 system is currently undergoing cyclic behavior. The character of the O – C residuals strongly resemble similar behavior of Algol binary systems (e.g., Soderhjelm 1980; Simon 1997). Numerous studies have been done of the O – C variations in Algol systems and the currently favored model is the O – C variations are brought about by magnetic cycling in the one of the binary components, in some ways similar to the 22-year solar magnetic cycle (Hall 1990). The orbital period changes we are seeing in EXO 0748–676, $|\Delta P_{orb}/P_{orb}| \sim 5 \times 10^{-7}$, are similar in magnitude to the observations of orbital period changes in Algol and RX CVn binaries (e.g., Hall 1990). If the observation of magnetic loop structures (Wolff et al. 2007) in the chromosphere of the secondary star in the EXO 0748–676 system is correct, then a magnetic cycling model for the O – C variations in EXO 0748–676 gains strong circumstantial support.

Before the *RXTE* era X-ray eclipse observations did not capture all the variations in the O – C residuals. Thus, no statement can be made about magnetic cycle time scales before the onset of *RXTE* observations. Once *RXTE* observations commenced in 1996, however, the richness of the O – C variations became apparent. The timescale for one cycle can be estimated as approximately twice $T_{b,2} - T_{b,1} \sim 4.8$ years from Table 1, or ~ 9.6 years for a complete cycle of the secondary star’s magnetic field *if* the cyclic field variations are similar to the polarity reversals experienced by the sun during one 22-year magnetic cycle. Exact predictions regarding when the system orbital period will change again are difficult, however, because we do not know exactly when the period shifted between $P_{\text{orb}2}$ and $P_{\text{orb}3}$. The O – C residuals near $n_{b,2}$ suggest that a gradual change in orbital period may have occurred.

In order to account for cyclic changes in the EXO 0748–676 orbital period, we must consider changes that occur on a time scale significantly less than the time scale for either mass exchange, spin-orbit coupling, or orbital circularization between the neutron star and secondary. We summarize here the model of Lanza et al. (1998) and Lanza & Rodonò (1999) where a detailed development of the magnetic cycling and orbital period modulation theory is given. We assume that the EXO 0748–676 binary consists of a magnetically active secondary star moving in the gravitational field of the neutron star, that the orbits are circular, and that the equatorial plane of the secondary lies roughly in the plane of the orbit. The secondary star in the EXO 0748–676 system is near $0.4 M_{\odot}$ implying that there is likely a convective envelope in the star and a resulting stellar magnetic field. The orbital angular momentum of the system will depend on the orbital radius, the orbital velocity and the mass of each stellar component. However, the cyclic changes of the magnetic field of the secondary induces cyclic changes in the secondary’s structure as magnetic pressure support in the convective layer varies. Thus, the gravitational quadrupole moment of the secondary star can be time-dependent and induce variable orbital motion. Since the mass of each component and orbital angular momentum are constant on the decadal time scales of interest here the orbital radius and the orbital velocity must undergo compensating changes as the gravitational field changes. But if the effective orbital radius changes, then, via Kepler’s law, the orbital period must also change. When the secondary’s gravitational quadrupole moment increases, the the gravitational pull from the secondary must also increase. This, in turn, will cause the two binary components to move toward each other causing the orbital velocity to increase and the orbital period to decrease. Conversely, as the quadrupole moment decreases the opposite effect occurs, again at constant orbital angular momentum, and the orbital period increases. All of this occurs on a time scale set by variations in the secondary’s magnetic field and not by the circularization or tidal coupling time scales that are expected to be significantly longer for such systems, and also not by the system mass exchange time scale. In a future publication we will report on a detailed comparison of the magnetic activity model with the

EXO 0748–676 system behavior.

4. Conclusions

We have analyzed 392 full X-ray eclipses from the EXO 0748–676 system observed by the *RXTE* satellite. We have carefully fitted a seven-parameter model to each eclipse light curve profile in order to determine the mid-eclipse timings and the errors on those timings. The observed O – C behavior of the EXO 0748–676 system we have found is much different than was expected when this project was started. The evolution of the binary system after more than 12 years of *RXTE* observations and eclipse timings is one of multiple orbital period epochs where the orbital period takes on distinct values that change rapidly. We have identified magnetic field cycling of the secondary star as the most likely cause of these O – C residual variations and given a brief description of how variations in the secondary’s magnetic field might bring about changes in the system orbital period. Also, the O – C diagram shows significant intrinsic jitter of various magnitudes during each separate epoch. This jitter most likely reflects subtle changes in the occulting edge of the secondary star caused by magnetic eruptions in the secondary star’s chromosphere.

We thank Jean Swank, Keith Jahoda, Alan Smale, Jacob Hartman, Deepto Chakrabarty, Mark Strickman, Neil Johnson, Peter Becker, Steve Howell, Craig Markwardt, and Philipp Podsiadlowski for important discussions. We thank Dr. Jeroen Homan for allowing us to look at proprietary data in advance of publication. We thank Evan Smith for invaluable help in scheduling the eclipse observations with *RXTE*. We thank an anonymous referee for a number of suggestions that helped to improve this paper. This work was supported by NASA Astrophysical Data Analysis Program, the NASA *RXTE* Guest Observer Program, and by the Office of Naval Research.

REFERENCES

- Bevington, P. R., & Robinson, D. K. 2003, Data reduction and error analysis for the physical sciences (3rd ed., McGraw-Hill, ISBN 0-07-247227-8)
- Cominsky, L. R., & Wood, K. S. 1989, *ApJ*, 337, 485
- Hall, D. S. 1990, in NATO ASIC Proc. 319: Active Close Binaries Proceedings, NATO Advanced Study Institute, 95–+

- Hertz, P., Wood, K. S., & Cominsky, L. 1995, *ApJ*, 438, 385
- Hertz, P., Wood, K. S., & Cominsky, L. R. 1997, *ApJ*, 486, 1000
- in’t Zand, J. J. M., Hulleman, F., Markwardt, C. B., Méndez, M., Kuulkers, E., Cornelisse, R., Heise, J., Strohmayer, T. E., & Verbunt, F. 2003, *A&A*, 406, 233
- Jahoda, K., Markwardt, C. B., Radeva, Y., Rots, A. H., Stark, M. J., Swank, J. H., Strohmayer, T. E., & Zhang, W. 2006, *ApJS*, 163, 401
- Jahoda, K., Swank, J. H., Giles, A. B., Stark, M. J., Strohmayer, T., Zhang, W., & Morgan, E. H. 1996, in *Proc. SPIE Vol. 2808*, p. 59-70, *EUV, X-Ray, and Gamma-Ray Instrumentation for Astronomy VII*, Oswald H. Siegmund; Mark A. Gummin; Eds., 59–70
- Koen, C. 1996, *MNRAS*, 283, 471
- Lanza, A. F., & Rodonò, M. 1999, *A&A*, 349, 887
- Lanza, A. F., Rodonoè, M., & Rosner, R. 1998, *MNRAS*, 296, 893
- Lewin, W. H. G., Hoffman, J. A., Doty, J., & Liller, W. 1976, *IAU Circ.*, 2994, 1
- Maeda, Y., Koyama, K., Sakano, M., Takeshima, T., & Yamauchi, S. 1996, *PASJ*, 48, 417
- Oosterbroek, T., Parmar, A. N., Sidoli, L., in’t Zand, J., & Heise, J. 2001, *A&A*, 376, 532
- Parmar, A. N., White, N. E., Giommi, P., & Gottwald, M. 1986, *ApJ*, 308, 199
- Porquet, D., Grosso, N., Goldwurm, A., Sakano, M., Belanger, G., Ferrando, P., Hasinger, G., Aschenbach, B., Predhel, P., Tanaka, Y., Genzel, R., Yusef-Zadeh, F., Warwick, R. S., & Melia, F. 2007, *The Astronomer’s Telegram*, 1058, 1
- Rappaport, S., Joss, P. C., & Webbink, R. F. 1982, *ApJ*, 254, 616
- Rots, A. H., Jahoda, K., Macomb, D. J., Kawai, N., Saito, Y., Kaspi, V. M., Lyne, A. G., Manchester, R. N., Backer, D. C., Somer, A. L., Marsden, D., & Rothschild, R. E. 1998, *ApJ*, 501, 749
- Sakano, M., Koyama, K., Murakami, H., Maeda, Y., & Yamauchi, S. 2002, *ApJS*, 138, 19
- Simon, V. 1997, *A&A*, 319, 886
- Soderhjelm, S. 1980, *A&A*, 89, 100

Wachter, S., Smale, A. P., & Bailyn, C. 2000, ApJ, 534, 367

Wolff, M. T., Hertz, P. L., Wood, K. S., Ray, P. S., & Bandyopadhyay, R. M. 2002, ApJ, 575, 384

Wolff, M. T., Wood, K. S., & Ray, P. S. 2007, ApJ, 668, L151

Table 1. *RXTE* Timing of Full EXO 0748–676 Eclipses

ObsID	Cycle Number	Mid-Eclipse Time (MJD;TDB)	Error (s)	Ingress Duration (s)	Totality Duration (s)	Egress Duration (s)	Pre-Ingress Count Rate (cnts s ⁻¹)	Totality Count Rate (cnts s ⁻¹)	Post-Egress Count Rate (cnts s ⁻¹)	Eclipse Fit χ^2_ν	Number of PCUs
10108-01-01-00	25702	50206.3747810	0.13	1.72(0.40)	508.26(0.44)	3.33(0.47)	112.6(1.3)	4.27(0.38)	123.6(1.4)	1.05	5
10108-01-02-00	25703	50206.5340983	0.12	1.29(0.29)	505.04(0.28)	2.82(0.34)	117.5(1.9)	2.90(0.35)	127.8(1.9)	1.07	5
10108-01-03-00	25704	50206.6934275	0.086	0.80(0.27)	504.35(0.42)	4.85(0.68)	107.3(1.8)	3.16(0.36)	120.8(1.8)	1.12	5
10108-01-04-00	25705	50206.8527675	0.30	3.46(0.65)	501.52(0.72)	11.01(0.83)	101.1(1.7)	3.71(0.36)	110.7(1.8)	1.16	5
10108-01-05-00	25706	50207.0121102	0.28	2.35(0.49)	503.14(0.48)	6.41(0.63)	99.4(1.7)	3.03(0.34)	105.1(1.8)	1.14	5
10068-03-02-00	26278	50298.1533303	0.16	3.44(0.59)	497.89(0.38)	5.15(0.53)	110.8(1.9)	-1.55(0.37)	138.7(2.0)	1.16	5
10108-01-06-00	26353	50310.1036665	0.21	1.86(0.61)	493.87(0.77)	10.9(1.4)	93.2(1.8)	7.12(0.44)	110.2(1.9)	1.21	5
10108-01-07-00	26354	50310.2630253	0.31	8.5(1.1)	493.38(0.72)	6.55(0.87)	121.5(1.9)	5.22(0.41)	136.7(2.0)	1.30	5
10108-01-08-00	26355	50310.4223693	0.29	6.44(0.90)	495.54(0.77)	5.64(0.74)	120.2(1.9)	5.85(0.37)	146.9(2.0)	1.15	5
10108-01-09-00	26356	50310.5817034	0.24	4.61(0.78)	495.94(0.52)	4.98(0.82)	99.6(2.0)	4.19(0.33)	108.2(1.7)	1.18	4
10108-01-07-01	26358	50310.9003923	0.22	7.8(1.0)	496.98(0.71)	5.18(0.68)	126.6(1.9)	4.59(0.40)	159.8(2.1)	1.31	5
10108-01-11-00	26654	50358.0644565	0.18	8.81(0.80)	504.79(0.56)	2.50(0.55)	86.6(1.6)	2.16(0.30)	96.2(1.6)	1.26	5
10108-01-12-00	26655	50358.2237829	0.19	5.47(0.58)	506.52(0.42)	3.01(0.45)	99.3(1.6)	3.12(0.31)	111.5(1.7)	1.36	5
10108-01-13-00	26656	50358.3831164	0.22	5.24(0.63)	504.88(0.45)	5.17(0.62)	101.5(1.6)	2.22(0.30)	124.3(1.8)	1.34	5
10108-01-14-00	26658	50358.7017946	0.30	9.6(1.2)	500.10(0.62)	9.4(1.1)	81.4(1.5)	1.61(0.30)	101.9(1.6)	1.33	5
10108-01-15-00	26659	50358.8611335	0.23	9.0(1.2)	503.34(0.70)	4.36(0.70)	97.3(1.6)	2.61(0.30)	113.8(1.7)	1.31	5
10108-01-15-01	26660	50359.0204769	0.24	7.8(1.1)	502.88(0.52)	5.59(0.73)	93.0(1.6)	1.18(0.29)	120.3(2.1)	1.23	5
20069-01-01-00	26999	50413.0360067	0.36	6.16(0.83)	501.61(0.78)	11.84(0.90)	89.7(1.6)	0.72(0.28)	106.0(1.6)	1.25	5
20069-01-02-00	27000	50413.1953059	0.35	7.7(1.0)	503.6(1.1)	13.3(1.4)	83.7(1.5)	0.65(0.29)	98.4(1.6)	1.33	5
20069-01-03-00	27001	50413.3546473	0.39	7.0(1.0)	504.95(0.81)	11.6(1.2)	84.0(1.5)	0.60(0.30)	105.2(1.7)	1.26	5
20069-01-05-00	27004	50413.8326765	0.44	11.5(1.5)	498.93(0.94)	11.4(1.6)	72.0(1.4)	1.34(0.30)	66.6(1.5)	1.23	5
20069-02-01-00	27336	50466.7328460	0.24	1.4(1.6)	511.22(0.58)	7.41(0.94)	71.2(1.0)	1.78(0.30)	90.0(1.2)	1.18	5
20069-02-02-00	27338	50467.0515284	0.49	3.90(0.76)	509.4(1.1)	7.68(0.85)	68.4(1.4)	0.40(0.27)	83.4(1.5)	1.21	5
20069-02-03-00	27339	50467.2108572	0.39	4.95(0.93)	508.2(1.1)	12.4(1.3)	73.5(1.4)	1.27(0.28)	88.2(1.5)	1.24	5
20069-02-04-00	27340	50467.3701831	0.26	2.60(0.75)	507.98(0.97)	11.8(1.5)	68.9(1.4)	1.71(0.28)	79.6(1.5)	1.28	5
20069-02-05-00	27341	50467.5295359	0.38	5.55(0.87)	507.76(0.83)	11.67(0.92)	71.8(1.5)	1.18(0.28)	96.2(1.6)	1.21	5
20069-03-01-00	27638	50514.8528420	0.42	7.8(1.3)	495.3(1.1)	7.5(1.1)	65.1(1.4)	-0.12(0.28)	77.9(1.5)	1.24	5
20069-03-02-00	27639	50515.0121643	0.27	3.37(0.70)	497.69(0.61)	7.62(0.82)	62.1(1.4)	0.14(0.27)	70.0(1.4)	1.14	5
20069-03-03-00	27640	50515.1715237	0.47	12.2(1.6)	494.0(1.2)	8.1(1.3)	54.7(1.2)	-0.85(0.24)	64.1(1.3)	1.21	4
20069-03-04-00	27641	50515.3308493	0.24	5.18(0.91)	497.58(0.49)	6.53(0.87)	84.8(1.5)	0.00(0.28)	93.3(1.5)	1.30	5
20069-03-05-00	27642	50515.4901699	0.11	1.84(0.42)	497.69(0.72)	5.81(0.92)	87.3(1.6)	-0.36(0.29)	83.8(1.5)	1.29	5
20069-04-01-00	27981	50569.5057230	0.29	6.39(0.99)	502.77(0.72)	9.3(1.1)	77.5(1.5)	0.22(0.29)	88.7(1.6)	1.11	5

Table 1—Continued

ObsID	Cycle Number	Mid-Eclipse Time (MJD;TDB)	Error (s)	Ingress Duration (s)	Totality Duration (s)	Egress Duration (s)	Pre-Ingress Count Rate (cnts s ⁻¹)	Totality Count Rate (cnts s ⁻¹)	Post-Egress Count Rate (cnts s ⁻¹)	Eclipse Fit χ_ν^2	Number of PCUs
20069-04-02-00	27982	50569.6650523	0.50	8.5(1.4)	501.25(0.95)	8.8(1.2)	66.1(1.4)	0.20(0.27)	79.8(1.5)	1.21	5
20069-04-03-00	27983	50569.8244043	0.34	7.6(1.0)	503.13(0.70)	6.29(0.84)	78.7(1.5)	0.09(0.26)	88.4(1.5)	1.14	5
20069-04-04-00	27984	50569.9837306	0.17	4.49(0.74)	502.15(0.75)	9.0(1.1)	78.9(1.5)	0.24(0.26)	84.9(1.5)	1.13	5
20069-04-05-00	27986	50570.3024234	0.25	3.74(0.70)	501.26(0.52)	6.38(0.90)	79.0(1.5)	0.36(0.28)	84.0(1.5)	1.16	5
20069-05-01-00	28331	50625.2738984	0.37	7.3(1.3)	498.6(1.0)	9.9(1.2)	71.1(1.5)	0.41(0.28)	80.6(1.5)	1.09	5
20069-05-02-00	28332	50625.4332600	0.47	8.3(1.3)	495.92(0.98)	8.5(1.1)	73.7(1.5)	-0.38(0.28)	82.0(1.5)	1.18	5
20069-05-03-00	28333	50625.5925880	0.49	7.7(1.0)	493.6(1.0)	13.3(1.4)	76.8(1.5)	-0.23(0.27)	84.5(1.5)	1.15	5
20069-05-04-00	28334	50625.7519383	0.41	5.94(0.82)	492.71(0.81)	10.96(0.94)	74.4(1.4)	0.39(0.27)	80.7(1.5)	1.16	5
20082-01-01-00	28636	50673.8719492	0.28	4.65(0.89)	498.93(0.59)	9.3(1.1)	96.3(1.7)	-1.78(0.36)	110.6(1.8)	1.22	5
20082-01-01-00	28637	50674.0312752	0.34	5.3(1.0)	500.35(0.84)	8.3(1.1)	96.5(1.8)	-3.66(0.37)	99.7(1.8)	1.24	5
20082-01-02-00	28662	50678.0147447	0.14	1.25(0.36)	498.41(0.59)	7.75(0.66)	96.8(1.8)	-3.34(0.40)	112.9(1.9)	1.20	5
20082-01-03-02	28690	50682.4761946	0.30	7.3(1.0)	500.48(0.79)	8.35(0.97)	104.0(1.8)	-1.84(0.37)	116.0(1.8)	1.28	5
20069-06-01-00	28976	50728.0468380	0.39	5.30(0.72)	504.01(0.71)	6.24(0.79)	85.1(1.6)	0.69(0.30)	89.9(1.6)	1.16	5
20069-06-02-00	28977	50728.2061501	0.23	6.78(0.91)	498.32(0.63)	7.3(1.0)	90.7(1.6)	0.51(0.28)	93.1(1.6)	1.22	5
20069-06-03-00	28978	50728.3654927	0.20	4.82(0.89)	500.46(0.52)	3.35(0.58)	87.7(1.5)	0.84(0.27)	94.7(1.6)	1.15	5
20069-06-04-00	28979	50728.5248396	0.32	5.54(0.68)	501.49(0.69)	8.87(0.77)	88.2(1.5)	-0.60(0.25)	94.2(1.6)	1.13	5
20069-06-05-00	28981	50728.8435022	0.34	7.1(1.1)	497.58(0.88)	7.18(0.92)	80.2(1.5)	0.55(0.29)	90.4(1.6)	1.22	5
30067-01-01-00	29610	50829.0669801	0.38	6.1(1.2)	497.37(0.91)	8.1(1.2)	59.9(1.3)	-0.49(0.26)	72.2(1.4)	1.26	4
30067-01-02-00	29611	50829.2263248	0.25	8.1(1.1)	500.02(0.69)	7.06(0.98)	75.3(1.4)	0.48(0.28)	89.3(1.5)	1.19	5
30067-01-03-00	29612	50829.3856366	0.41	5.7(1.0)	498.82(0.92)	11.3(1.3)	81.3(1.5)	-0.61(0.29)	91.3(1.6)	1.34	5
30067-01-04-00	29613	50829.5449867	0.28	3.55(0.69)	499.57(0.57)	6.81(0.70)	76.5(1.4)	0.13(0.28)	91.5(1.5)	1.30	5
30067-01-05-00	29614	50829.7043161	0.28	6.3(1.0)	498.55(0.58)	9.0(1.1)	59.0(1.3)	-0.11(0.25)	66.2(1.4)	1.19	4
30067-02-01-00	29966	50885.7912899	0.36	7.3(1.2)	499.22(0.76)	6.8(1.1)	78.8(1.4)	-0.33(0.29)	78.2(1.5)	1.34	5
30067-02-02-00	29967	50885.9506117	0.25	4.67(0.87)	501.04(0.72)	9.2(1.1)	84.1(1.5)	0.72(0.27)	79.5(1.5)	1.15	5
30067-02-03-00	29968	50886.1099626	0.22	4.78(0.91)	499.76(0.46)	8.0(1.1)	81.4(1.5)	-0.07(0.31)	85.2(1.5)	1.26	5
30067-02-04-00	29970	50886.4286321	0.38	2.61(0.88)	496.6(1.1)	14.4(1.7)	57.5(1.3)	0.10(0.27)	67.9(1.4)	1.26	4
30067-02-05-00	29971	50886.5879661	0.29	2.84(0.69)	498.98(0.67)	10.9(1.3)	80.8(1.5)	0.12(0.31)	85.7(1.6)	1.31	5
30067-03-01-00	30636	50992.5475844	0.37	5.28(0.94)	503.47(0.75)	9.0(1.1)	84.5(1.5)	0.40(0.28)	91.2(1.5)	1.32	5
30067-03-02-00	30637	50992.7069370	0.52	8.5(1.2)	501.99(0.89)	8.9(1.1)	83.7(1.5)	0.74(0.29)	92.2(1.6)	1.33	5
30067-03-03-00	30638	50992.8662837	0.39	6.5(1.1)	504.1(1.0)	7.0(1.2)	64.5(1.4)	-0.00(0.26)	66.1(1.4)	1.19	4
30067-03-04-00	30640	50993.1849496	0.29	7.1(1.1)	506.02(0.75)	4.85(0.79)	87.6(1.6)	0.45(0.31)	88.7(1.6)	1.24	5
30067-03-05-00	30641	50993.3442843	0.24	4.87(0.98)	504.41(0.97)	8.7(1.1)	90.7(1.6)	0.45(0.31)	98.9(1.6)	1.39	5

Table 1—Continued

ObsID	Cycle Number	Mid-Eclipse Time (MJD;TDB)	Error (s)	Ingress Duration (s)	Totality Duration (s)	Egress Duration (s)	Pre-Ingress Count Rate (cnts s ⁻¹)	Totality Count Rate (cnts s ⁻¹)	Post-Egress Count Rate (cnts s ⁻¹)	Eclipse Fit χ_ν^2	Number of PCUs
30067-04-01-00	30997	51050.0685711	0.24	5.0(1.2)	495.76(0.65)	7.08(0.99)	78.6(1.5)	0.40(0.30)	91.4(1.6)	1.27	5
30067-04-02-00	30998	51050.2279167	0.36	6.7(1.1)	495.16(0.75)	7.4(1.1)	79.6(1.5)	0.42(0.28)	85.4(1.5)	1.22	5
30067-04-04-00	31000	51050.5465627	0.27	5.44(0.80)	502.40(0.66)	5.61(0.85)	89.3(1.5)	0.49(0.27)	99.1(1.6)	1.21	5
30067-04-05-00	31001	51050.7058907	0.51	5.42(0.92)	500.5(1.1)	11.2(1.1)	54.3(1.2)	-0.35(0.21)	57.0(1.2)	1.15	3
30067-05-01-00	31292	51097.0732381	0.19	7.26(0.89)	493.40(0.50)	6.26(0.92)	92.9(1.6)	0.14(0.29)	96.8(1.6)	1.12	5
30067-05-02-00	31293	51097.2325594	0.20	4.36(0.74)	494.58(0.46)	6.67(0.77)	95.8(1.9)	-0.09(0.26)	91.4(1.6)	1.03	5
30067-05-03-00	31294	51097.3919042	0.24	5.45(0.81)	497.56(0.53)	3.38(0.59)	86.1(1.5)	0.48(0.26)	94.6(1.6)	1.07	5
30067-05-04-00	31295	51097.5512344	0.12	1.58(0.44)	495.37(0.41)	7.54(0.70)	92.0(1.5)	-0.38(0.26)	97.3(1.6)	1.16	5
30067-05-05-00	31297	51097.8698983	0.31	3.87(0.60)	496.27(0.71)	7.71(0.84)	93.6(1.6)	-0.24(0.27)	98.9(1.6)	1.07	5
30067-06-01-00	31665	51156.5062370	0.24	12.4(1.1)	496.38(0.70)	3.99(0.61)	102.6(1.6)	-0.19(0.25)	107.8(1.6)	1.09	5
30067-06-02-00	31666	51156.6655607	0.097	11.8(1.2)	495.51(0.25)	3.50(0.76)	94.6(1.6)	-0.48(0.27)	100.0(1.6)	1.10	5
30067-06-03-00	31668	51156.9842472	0.24	12.4(1.4)	495.01(0.63)	2.73(0.61)	75.4(1.5)	0.44(0.27)	69.5(1.4)	1.17	5
30067-06-04-00	31669	51157.1435806	0.15	11.4(1.0)	494.2(1.3)	1.64(0.50)	52.61(0.90)	1.01(0.23)	53.35(0.91)	1.05	4
30067-06-05-00	31670	51157.3029182	0.25	9.7(1.0)	496.90(0.75)	4.87(0.84)	56.5(1.2)	0.34(0.23)	68.4(1.4)	1.11	4
40039-01-01-00	31955	51202.7141877	0.41	9.2(1.2)	496.39(0.84)	6.08(0.97)	68.3(1.4)	-0.70(0.24)	68.5(1.4)	1.03	4
40039-01-02-00	31956	51202.8735334	0.21	10.70(0.77)	496.12(0.70)	3.15(0.58)	90.0(1.6)	-0.62(0.26)	89.0(1.5)	1.06	5
40039-01-04-00	31959	51203.3515343	0.24	8.12(0.92)	498.55(0.54)	3.34(0.54)	99.3(1.6)	-1.21(0.26)	93.6(1.6)	1.08	5
40039-01-05-00	31960	51203.5108714	0.19	6.75(0.61)	499.14(0.42)	3.77(0.57)	97.9(1.6)	-0.48(0.25)	98.3(1.6)	1.13	5
40039-02-01-00	32305	51258.4824762	0.40	8.6(1.3)	496.89(0.82)	8.0(1.1)	64.5(1.4)	-0.46(0.25)	73.0(1.4)	1.16	4
40039-02-02-00	32306	51258.6418008	0.27	7.1(1.1)	498.06(0.57)	5.71(0.85)	67.8(1.4)	-0.76(0.24)	72.0(1.4)	1.17	4
40039-02-03-00	32308	51258.9604765	0.27	6.70(0.90)	498.20(0.68)	3.71(0.74)	49.4(1.1)	-0.98(0.20)	47.1(1.1)	1.23	3
40039-02-04-00	32309	51259.1197864	0.41	5.8(1.7)	495.7(1.0)	10.5(1.7)	29.42(0.94)	-1.63(0.17)	33.77(0.97)	1.20	2
40039-02-05-00	32310	51259.2791599	0.12	4.96(0.83)	502.07(0.31)	3.73(0.82)	70.3(1.3)	-0.38(0.22)	71.7(1.4)	1.11	4
40039-03-01-00	32624	51309.3111982	0.23	4.24(0.64)	493.96(0.53)	8.43(0.74)	79.1(1.5)	1.27(0.26)	92.5(1.5)	1.23	4
40039-03-02-00	32625	51309.4705716	0.29	7.9(1.0)	496.65(0.74)	6.25(0.83)	84.7(1.5)	0.82(0.27)	91.5(1.5)	1.31	4
40039-03-03-00	32627	51309.7892236	0.11	7.25(0.79)	492.75(0.57)	7.88(0.82)	90.0(1.5)	1.71(0.25)	88.7(1.8)	1.22	4
40039-03-04-00	32628	51309.9485712	0.23	7.38(0.75)	496.42(0.46)	3.89(0.62)	78.6(1.4)	0.64(0.22)	73.1(1.4)	1.20	3
40039-03-05-00	32629	51310.1079167	0.35	6.63(0.90)	498.16(0.79)	9.8(1.1)	71.3(1.3)	0.35(0.21)	75.8(1.4)	1.23	3
40039-04-01-00	32964	51363.4860776	0.23	7.5(1.0)	498.06(0.48)	6.06(0.77)	75.1(1.4)	0.37(0.24)	86.2(1.5)	1.19	4
40039-04-02-00	32965	51363.6454133	0.17	11.1(1.4)	497.1(1.2)	2.06(0.58)	59.7(1.2)	-1.09(0.20)	63.9(1.3)	1.20	3
40039-04-03-00	32966	51363.8047882	0.21	12.3(1.8)	500.95(0.72)	3.22(0.78)	46.1(1.1)	-0.41(0.22)	44.3(1.1)	1.18	3
40039-04-04-00	32968	51364.1234238	0.19	7.7(1.2)	495.88(0.79)	3.15(0.79)	63.5(1.4)	2.06(0.33)	78.5(1.5)	1.20	4

Table 1—Continued

ObsID	Cycle Number	Mid-Eclipse Time (MJD;TDB)	Error (s)	Ingress Duration (s)	Totality Duration (s)	Egress Duration (s)	Pre-Ingress Count Rate (cnts s ⁻¹)	Totality Count Rate (cnts s ⁻¹)	Post-Egress Count Rate (cnts s ⁻¹)	Eclipse Fit χ_ν^2	Number of PCUs
40039-05-02-00	33266	51411.6061289	0.39	10.5(1.2)	488.4(1.0)	5.09(0.79)	83.2(1.4)	-0.45(0.23)	82.4(1.5)	1.18	4
40039-05-03-00	33267	51411.7654843	0.39	2.64(0.82)	498.52(0.82)	3.76(0.78)	64.5(1.4)	-0.19(0.24)	66.8(1.4)	1.22	4
40039-05-04-00	33269	51412.0840985	0.23	6.7(1.0)	493.33(0.59)	3.4(1.0)	66.9(1.4)	0.12(0.26)	47.0(1.1)	1.27	4
40039-05-05-00	33270	51412.2434689	0.54	4.8(1.3)	490.5(1.2)	4.3(1.4)	31.71(0.94)	-1.50(0.17)	31.86(0.94)	1.28	2
40039-06-02-00	33622	51468.3303763	0.49	10.0(1.9)	486.2(1.3)	5.3(1.5)	41.5(1.1)	0.27(0.21)	40.7(1.1)	1.29	3
40039-06-03-00	33623	51468.4897333	0.32	4.2(1.0)	494.50(0.67)	6.3(1.2)	73.7(1.5)	2.02(0.29)	63.0(1.3)	1.33	5
40039-06-04-00	33625	51468.8084029	0.57	4.8(1.1)	490.6(1.1)	18.2(2.0)	59.1(1.3)	1.81(0.30)	67.1(1.4)	1.36	5
50045-01-01-00	34647	51631.6516385	0.22	4.21(0.76)	498.11(0.56)	6.07(0.81)	99.5(1.6)	3.48(0.28)	108.0(1.6)	1.22	5
50045-01-02-00	34648	51631.8109671	0.25	6.3(1.0)	497.64(0.55)	7.32(0.92)	96.4(1.6)	2.88(0.28)	117.4(1.7)	1.24	5
50045-01-03-00	34649	51631.9703171	0.44	9.7(1.5)	495.5(1.0)	7.7(1.4)	42.9(1.1)	-0.47(0.18)	45.2(1.1)	1.23	2
50045-01-05-00	34652	51632.4483046	0.27	6.12(0.82)	497.40(0.80)	7.84(0.82)	113.8(1.7)	2.55(0.29)	134.1(1.8)	1.20	5
50045-02-01-00	34934	51677.3815806	0.17	9.4(1.1)	499.6(1.1)	2.28(0.49)	79.3(1.5)	1.34(0.25)	86.4(1.5)	1.15	4
50045-02-02-00	34935	51677.5408963	0.18	5.39(0.57)	489.66(0.39)	4.12(0.57)	97.8(1.6)	1.30(0.25)	96.1(1.6)	1.23	4
50045-02-03-00	34937	51677.8595585	0.20	3.57(0.85)	492.27(0.41)	4.65(0.86)	42.9(1.0)	-1.69(0.16)	48.4(1.1)	1.41	2
50045-02-04-00	34938	51678.0189231	0.22	3.08(0.70)	493.32(0.68)	10.39(0.95)	59.9(1.3)	-0.33(0.21)	67.8(1.3)	1.22	3
50045-02-05-00	34939	51678.1782362	0.083	1.82(0.87)	490.46(0.35)	4.53(0.80)	62.1(1.3)	-0.06(0.21)	72.3(1.3)	1.33	3
50045-03-01-00	35304	51736.3365376	0.21	1.91(0.45)	495.62(0.81)	8.4(1.0)	90.0(1.5)	1.32(0.27)	89.2(1.5)	1.23	4
50045-03-03-00	35306	51736.6552331	0.21	4.37(0.65)	495.65(0.50)	5.95(0.80)	125.8(1.8)	2.16(0.32)	131.1(1.8)	1.22	5
50045-03-04-00	35308	51736.9739256	0.23	10.14(0.95)	495.10(0.55)	4.72(0.75)	105.5(1.7)	0.24(0.27)	108.3(1.7)	1.19	4
50045-04-01-00	35610	51785.0939116	0.29	9.1(1.1)	492.98(0.69)	7.5(1.0)	93.9(1.6)	0.90(0.28)	98.0(1.6)	1.25	4
50045-04-02-00	35611	51785.2532316	0.27	9.9(1.2)	490.54(0.62)	3.86(0.62)	93.4(1.6)	0.88(0.28)	97.4(1.6)	1.20	4
50045-04-03-00	35612	51785.4125829	0.24	5.30(0.60)	496.07(0.61)	6.37(0.59)	108.1(1.7)	3.57(0.35)	141.9(1.9)	1.23	5
50045-04-04-00	35613	51785.5718809	0.21	5.24(0.56)	493.02(0.44)	5.50(0.59)	96.8(1.6)	0.27(0.25)	102.4(1.6)	1.12	4
50045-04-05-00	35614	51785.7312167	0.19	4.75(0.56)	488.91(0.45)	11.72(0.73)	121.4(1.8)	2.09(0.30)	121.9(1.8)	1.30	5
50045-04-06-00	35615	51785.8905899	0.29	7.10(0.97)	492.46(0.72)	8.5(1.1)	99.1(1.6)	2.45(0.33)	100.5(1.6)	1.44	5
50045-05-01-00	35948	51838.9500828	0.20	7.9(1.1)	493.40(0.54)	3.21(0.62)	90.1(1.6)	0.72(0.28)	105.3(1.6)	1.25	4
50045-05-02-00	35949	51839.1093888	0.11	6.73(0.87)	489.84(0.51)	6.30(0.94)	88.0(1.6)	0.40(0.27)	97.0(1.6)	1.18	4
50045-05-03-00	35950	51839.2687578	0.24	7.81(0.76)	492.44(0.73)	4.42(0.62)	92.0(1.5)	2.06(0.26)	96.1(1.6)	1.11	4
50045-05-04-00	35951	51839.4281136	0.18	8.74(0.72)	493.1(1.2)	2.84(0.51)	84.7(1.5)	1.07(0.27)	89.6(1.6)	1.20	4
50045-05-05-00	35952	51839.5873993	0.30	7.5(1.1)	489.80(0.90)	4.82(0.84)	64.2(1.3)	-0.77(0.23)	67.7(1.3)	1.23	3
50045-06-01-00	36305	51895.8336172	0.29	5.88(0.84)	485.22(0.59)	14.8(1.0)	74.7(1.4)	0.19(0.27)	85.1(1.5)	1.28	4
50045-06-03-00	36307	51896.1522971	0.32	7.81(0.87)	490.90(0.71)	6.45(0.75)	75.9(1.5)	0.49(0.27)	92.6(1.5)	1.17	4

Table 1—Continued

ObsID	Cycle Number	Mid-Eclipse Time (MJD;TDB)	Error (s)	Ingress Duration (s)	Totality Duration (s)	Egress Duration (s)	Pre-Ingress Count Rate (cnts s ⁻¹)	Totality Count Rate (cnts s ⁻¹)	Post-Egress Count Rate (cnts s ⁻¹)	Eclipse Fit χ_ν^2	Number of PCUs
50045-06-04-00	36309	51896.4709934	0.27	6.06(0.89)	490.52(0.68)	7.62(0.98)	86.1(1.5)	0.25(0.27)	95.6(1.6)	1.27	4
60047-01-01-00	36924	51994.4637081	0.19	5.20(0.62)	490.88(0.40)	5.64(0.63)	92.3(1.6)	1.00(0.28)	99.1(1.6)	1.17	4
60047-01-06-00	36925	51994.6230433	0.20	3.37(0.55)	490.79(0.46)	8.04(0.82)	113.3(1.7)	2.10(0.30)	122.7(1.8)	1.18	5
60047-01-02-00	36926	51994.7823900	0.13	2.66(0.42)	489.81(0.27)	4.13(0.51)	112.5(1.7)	1.44(0.29)	119.1(1.7)	1.17	5
60047-01-03-00	36927	51994.9417268	0.12	4.91(0.82)	491.59(0.34)	2.73(0.65)	90.1(1.5)	0.72(0.25)	95.4(1.6)	1.13	4
60047-01-04-00	36928	51995.1010513	0.37	7.88(0.96)	487.09(0.96)	8.00(0.91)	85.9(1.5)	-0.09(0.25)	90.8(1.5)	1.13	4
60047-01-05-00	36929	51995.2603950	0.28	4.22(0.68)	489.17(0.78)	6.57(0.73)	86.5(1.5)	-0.17(0.27)	93.5(1.5)	1.26	4
60047-02-01-00	37268	52049.2758941	0.37	6.90(0.94)	495.72(0.94)	3.89(0.66)	80.5(1.5)	1.13(0.27)	89.8(1.5)	1.10	4
60047-02-06-00	37269	52049.4352135	0.25	2.31(0.59)	495.05(0.53)	4.88(0.80)	67.2(1.3)	0.11(0.23)	71.0(1.4)	1.14	3
60047-02-02-00	37270	52049.5945635	0.27	4.90(0.80)	493.54(0.66)	8.39(0.94)	60.5(1.3)	0.70(0.22)	61.2(1.3)	1.11	3
60047-02-03-00	37271	52049.7539264	0.89	10.3(1.3)	489.5(1.5)	6.6(1.1)	39.4(1.0)	-0.96(0.18)	43.9(1.1)	1.09	2
60047-02-04-00	37272	52049.9132407	0.40	7.86(0.95)	490.0(1.0)	6.17(0.81)	55.7(1.3)	-0.27(0.22)	71.5(1.3)	1.17	3
60047-02-05-00	37273	52050.0725840	0.30	6.94(0.89)	494.1(1.0)	5.59(0.83)	56.9(1.3)	-0.02(0.23)	66.5(1.3)	1.21	3
60047-03-01-00	37574	52098.0332385	0.32	3.47(0.90)	488.65(0.68)	4.1(1.5)	46.32(0.84)	1.51(0.24)	38.42(0.81)	1.21	3
60047-03-02-00	37575	52098.1925819	0.37	4.27(0.88)	489.54(0.67)	10.3(1.2)	74.4(1.4)	0.32(0.24)	70.6(1.4)	1.20	3
60047-03-03-00	37577	52098.5112804	0.21	2.86(0.77)	494.46(0.46)	4.73(0.72)	67.4(1.3)	0.42(0.22)	72.5(1.4)	1.15	3
60047-03-04-00	37578	52098.6706157	0.25	2.60(0.67)	492.51(0.53)	3.33(0.66)	56.7(1.3)	-0.07(0.25)	68.0(1.4)	1.14	3
60047-03-05-00	37579	52098.8299349	0.27	4.68(0.97)	489.74(0.60)	4.92(0.82)	63.3(1.3)	0.14(0.22)	70.3(1.3)	1.18	3
60047-04-01-00	37912	52151.8894007	0.24	7.85(0.73)	490.23(0.50)	4.94(0.55)	115.5(1.7)	0.26(0.24)	121.9(1.7)	1.04	4
60047-04-02-00	37913	52152.0487400	0.20	3.74(0.71)	489.12(0.45)	2.83(0.49)	84.0(1.4)	0.01(0.22)	90.6(1.5)	1.06	3
60047-04-03-00	37915	52152.3673833	0.23	4.91(0.58)	493.58(0.47)	4.51(0.56)	116.4(1.7)	0.34(0.24)	119.8(1.7)	1.06	4
60047-04-04-00	37916	52152.5267751	0.19	4.30(0.50)	493.55(0.41)	3.91(0.50)	91.3(1.5)	-0.26(0.24)	99.8(1.6)	1.06	3
60047-04-05-00	37917	52152.6861005	0.18	5.45(0.62)	491.57(0.38)	4.49(0.63)	93.6(1.5)	0.01(0.21)	100.0(1.5)	1.08	3
60047-05-01-00	38257	52206.8609441	0.095	2.29(0.40)	492.64(0.27)	4.86(0.75)	86.7(1.5)	-0.80(0.24)	92.0(1.5)	1.05	4
60047-05-02-00	38258	52207.0202676	0.21	4.45(0.88)	489.73(0.47)	1.74(0.59)	83.1(1.5)	-0.28(0.25)	83.0(1.5)	1.08	4
60047-05-03-00	38259	52207.1796068	0.26	4.49(0.81)	490.61(0.55)	4.14(0.62)	67.1(1.3)	-0.63(0.21)	72.3(1.4)	1.03	3
60047-05-04-00	38260	52207.3389651	0.22	4.41(0.53)	495.52(0.44)	3.20(0.51)	75.0(1.4)	-0.73(0.22)	69.6(1.4)	1.03	3
60047-05-05-00	38261	52207.4982731	0.33	2.67(0.60)	490.35(0.58)	10.9(1.2)	60.8(1.3)	-1.06(0.21)	68.4(1.3)	1.13	3
60047-06-01-00	38583	52258.8050188	0.37	5.39(0.92)	491.79(0.84)	11.0(1.1)	79.9(1.4)	1.70(0.27)	62.4(1.4)	1.21	4
60047-06-02-00	38584	52258.9643603	0.16	7.1(1.1)	489.33(0.65)	3.8(1.1)	71.4(1.4)	-0.32(0.24)	41.3(1.1)	1.33	3
60047-06-03-00	38585	52259.1237071	0.31	9.1(1.4)	486.01(0.79)	10.1(1.6)	43.8(1.1)	-0.22(0.20)	40.9(1.1)	1.13	2
60047-06-04-00	38587	52259.4423910	0.21	3.27(0.63)	495.11(0.44)	3.13(0.53)	67.6(1.3)	-0.43(0.21)	81.9(1.4)	1.16	3

Table 1—Continued

ObsID	Cycle Number	Mid-Eclipse Time (MJD;TDB)	Error (s)	Ingress Duration (s)	Totality Duration (s)	Egress Duration (s)	Pre-Ingress Count Rate (cnts s ⁻¹)	Totality Count Rate (cnts s ⁻¹)	Post-Egress Count Rate (cnts s ⁻¹)	Eclipse Fit χ_ν^2	Number of PCUs
60047-06-05-00	38588	52259.6017385	0.39	11.0(1.4)	489.10(0.88)	8.1(1.1)	59.0(1.3)	0.50(0.23)	75.9(1.4)	1.15	3
70048-01-01-00	38847	52300.8701732	0.25	6.0(1.0)	487.58(0.56)	10.4(1.3)	58.4(1.3)	0.13(0.22)	67.8(1.3)	1.16	3
70048-01-02-00	38848	52301.0295415	0.37	7.4(1.2)	490.6(1.0)	5.3(1.0)	54.9(1.2)	-0.17(0.23)	60.6(1.3)	1.21	3
70048-01-04-00	38850	52301.3482241	0.24	11.5(1.5)	487.71(0.98)	6.5(1.3)	60.4(1.3)	0.05(0.26)	62.4(1.3)	1.16	3
70048-02-01-00	39156	52350.1055483	0.35	7.8(1.2)	492.58(0.82)	7.00(0.95)	68.8(1.4)	0.68(0.25)	79.9(1.4)	1.17	3
70048-02-02-00	39157	52350.2648877	0.41	9.64(0.94)	493.78(0.89)	5.18(0.84)	66.3(1.3)	0.36(0.23)	71.1(1.4)	1.16	3
70048-02-03-00	39160	52350.7429082	0.23	4.82(0.87)	490.59(0.53)	8.19(0.97)	73.4(1.4)	-0.38(0.23)	72.9(1.4)	1.18	3
70048-03-01-00	39326	52377.1929516	0.23	4.35(0.83)	488.16(0.48)	12.7(1.3)	86.7(1.5)	1.88(0.30)	99.6(1.7)	1.28	5
70048-03-04-00	39353	52381.4951036	0.38	8.2(1.3)	488.99(0.84)	7.0(1.5)	67.2(1.4)	1.03(0.29)	59.8(1.3)	1.32	4
70048-03-02-00	39370	52384.2038238	0.46	6.90(0.88)	486.43(0.97)	7.69(0.90)	67.5(1.3)	0.45(0.23)	70.7(1.3)	1.23	3
70048-03-03-00	39372	52384.5225066	0.30	9.1(1.1)	486.53(0.60)	9.05(0.99)	92.8(1.6)	1.51(0.30)	111.7(3.3)	1.18	4
70048-04-01-00	39565	52415.2746810	0.26	7.75(0.93)	490.77(0.53)	8.0(1.0)	97.1(1.5)	0.82(0.26)	98.3(1.6)	1.22	4
70048-04-02-00	39567	52415.5933532	0.28	9.0(1.6)	488.50(0.56)	7.0(1.5)	42.9(1.1)	-0.70(0.20)	47.3(1.1)	1.29	2
70048-04-03-00	39568	52415.7527081	0.31	6.8(1.4)	490.94(0.86)	3.85(0.98)	41.5(1.1)	-0.63(0.21)	47.2(1.2)	1.20	2
70048-04-04-00	39569	52415.9120260	0.56	5.5(1.0)	488.5(1.4)	8.7(1.1)	45.1(1.0)	0.91(0.19)	49.6(1.1)	1.16	2
70048-05-01-00	39812	52454.6311072	0.23	8.70(0.87)	486.77(0.67)	7.51(0.82)	83.0(1.5)	1.72(0.26)	93.6(1.5)	1.19	4
70048-05-02-00	39813	52454.7904410	0.40	8.60(0.94)	486.7(1.1)	10.09(0.91)	74.7(1.4)	0.50(0.26)	85.6(1.5)	1.27	3
70048-05-03-00	39814	52454.9497870	0.39	9.8(1.1)	487.3(1.0)	6.0(1.0)	57.9(1.3)	0.54(0.24)	55.5(1.3)	1.17	3
70048-05-04-00	39815	52455.1090982	0.33	4.75(0.74)	490.79(0.76)	8.31(0.92)	84.0(1.5)	0.78(0.26)	93.4(1.5)	1.25	4
70048-06-01-00	40003	52485.0646216	0.29	7.7(1.3)	489.75(0.56)	6.26(0.95)	71.0(1.5)	0.36(0.26)	92.7(1.5)	1.28	4
70048-06-02-00	40015	52486.9766590	0.16	3.41(0.59)	492.31(0.50)	7.46(0.98)	73.1(1.3)	-0.14(0.22)	75.0(1.4)	1.18	3
70048-06-04-00	40022	52488.0920171	0.32	3.95(0.83)	490.87(0.84)	8.8(1.3)	75.4(1.4)	0.77(0.24)	71.8(1.3)	1.22	3
70048-07-01-00	40209	52517.8881892	0.24	4.27(0.60)	490.94(0.54)	12.64(0.83)	88.8(1.5)	0.71(0.26)	102.4(1.9)	1.20	4
70048-07-02-00	40211	52518.2068578	0.35	5.7(1.1)	492.02(0.72)	9.4(1.2)	58.2(1.3)	-0.03(0.23)	65.5(1.3)	1.22	3
70048-07-03-00	40212	52518.3662047	0.37	4.9(1.2)	495.33(0.92)	9.0(1.3)	46.2(1.2)	-0.32(0.23)	46.0(1.1)	1.27	3
70048-09-01-00	40642	52586.8814332	0.29	8.92(0.91)	489.00(0.60)	12.33(0.98)	73.7(1.4)	-0.49(0.23)	75.2(1.4)	1.16	3
70048-09-02-00	40647	52587.6780944	0.56	10.7(1.4)	487.2(1.4)	16.6(1.6)	44.7(1.1)	-0.86(0.19)	40.7(1.1)	1.13	2
70048-09-03-00	40654	52588.7934799	0.34	2.35(0.89)	490.26(0.76)	9.9(1.7)	39.4(1.1)	-0.54(0.23)	41.3(1.1)	1.25	2
70048-09-04-00	40661	52589.9088435	0.33	7.3(1.1)	488.27(0.82)	14.9(1.6)	63.6(1.3)	-0.13(0.24)	68.6(1.4)	1.10	3
60042-03-01-01	40805	52612.8534830	0.40	6.45(0.98)	491.9(1.0)	6.5(1.1)	80.4(1.5)	0.89(0.27)	75.3(1.4)	1.30	4
60042-03-01-02	40812	52613.9688703	0.32	9.46(0.81)	491.34(0.68)	4.11(0.59)	81.6(1.5)	0.26(0.25)	82.7(1.5)	1.23	4
60042-03-02-02	40824	52615.8809097	0.25	3.25(0.64)	491.58(0.94)	5.81(0.82)	59.6(1.3)	-0.50(0.23)	51.8(1.2)	1.26	3

Table 1—Continued

ObsID	Cycle Number	Mid-Eclipse Time (MJD;TDB)	Error (s)	Ingress Duration (s)	Totality Duration (s)	Egress Duration (s)	Pre-Ingress Count Rate (cnts s ⁻¹)	Totality Count Rate (cnts s ⁻¹)	Post-Egress Count Rate (cnts s ⁻¹)	Eclipse Fit χ^2_ν	Number of PCUs
60042-03-02-01	40830	52616.8369297	0.23	7.36(0.92)	491.51(0.52)	5.39(0.85)	69.4(1.4)	0.44(0.26)	66.9(1.4)	1.13	4
60042-03-02-01	40831	52616.9962682	0.27	3.43(0.78)	491.60(0.85)	5.2(1.2)	48.9(1.2)	0.30(0.21)	48.8(1.2)	1.09	3
70048-10-01-00	40854	52620.6610283	0.30	3.50(0.90)	487.6(1.0)	9.9(1.5)	65.2(1.3)	-0.12(0.24)	60.3(1.3)	1.34	3
70048-10-02-00	40856	52620.9797091	0.21	1.30(0.40)	491.20(0.51)	7.9(1.1)	71.4(1.4)	0.26(0.27)	76.8(1.4)	1.28	4
70048-10-03-00	40857	52621.1390479	0.28	6.9(1.1)	490.61(0.59)	7.9(1.3)	57.1(1.2)	-0.22(0.22)	58.1(1.3)	1.21	3
70048-10-04-00	40858	52621.2983889	0.34	12.5(1.5)	491.32(0.70)	6.7(1.1)	61.2(1.3)	-0.41(0.22)	60.9(1.3)	1.18	3
70048-11-01-00	41089	52658.1054102	0.27	3.31(0.63)	492.62(0.64)	6.89(0.77)	61.9(1.3)	-0.44(0.23)	63.3(1.3)	1.16	3
70048-11-02-00	41090	52658.2647627	0.35	6.1(1.0)	498.04(0.75)	2.79(0.76)	61.9(1.3)	-0.09(0.22)	64.7(1.3)	1.07	3
70048-11-03-00	41091	52658.4241091	0.18	4.59(0.78)	495.49(0.41)	1.76(0.65)	85.1(1.5)	-0.08(0.26)	85.1(1.5)	1.20	4
70048-11-04-00	41092	52658.5834356	0.19	2.96(0.50)	494.38(0.55)	2.15(0.50)	80.3(1.4)	0.35(0.24)	82.4(1.5)	1.16	4
70047-01-01-13	41275	52687.7422070	0.40	2.78(0.90)	488.9(1.1)	12.5(1.7)	54.9(1.0)	0.14(0.29)	66.7(1.1)	0.96	3
70047-01-01-14	41280	52688.5389252	0.22	3.7(1.0)	491.35(0.55)	4.30(0.78)	63.9(1.4)	-1.77(0.28)	68.4(1.4)	1.15	3
70047-02-01-13	41284	52689.1762590	0.21	1.57(0.54)	491.28(0.70)	5.43(0.75)	66.6(1.4)	-1.55(0.27)	65.1(1.4)	1.10	3
70047-01-01-15	41287	52689.6542820	0.17	2.86(0.91)	494.3(1.9)	3.90(0.81)	70.2(1.5)	-1.52(0.30)	71.0(1.5)	1.08	3
70048-12-01-00	41462	52717.5383657	0.27	4.55(0.80)	493.81(0.54)	4.73(0.78)	57.6(1.3)	-1.15(0.22)	62.0(1.3)	1.09	3
70048-12-02-00	41463	52717.6977083	0.25	6.15(0.77)	492.70(0.52)	5.86(0.74)	85.4(1.5)	-0.61(0.23)	87.2(1.5)	1.11	4
70048-12-03-00	41464	52717.8570454	0.29	4.45(0.66)	495.19(0.55)	3.93(0.62)	67.3(1.3)	-0.82(0.22)	68.0(1.3)	1.17	3
70048-12-04-00	41465	52718.0163935	0.28	6.3(1.0)	494.03(0.70)	4.95(0.86)	61.8(1.3)	-0.90(0.21)	63.7(1.3)	1.12	3
70048-13-01-00	42101	52819.3552215	0.36	14.68(0.99)	492.07(0.95)	4.67(0.73)	88.0(1.5)	-0.28(0.26)	91.4(1.5)	1.29	4
70048-13-02-00	42102	52819.5145652	0.20	8.9(1.0)	497.28(0.52)	4.76(0.72)	80.0(1.5)	0.32(0.26)	82.4(1.5)	1.23	4
70048-13-04-00	42104	52819.8332456	0.29	10.3(1.1)	498.25(0.65)	7.8(1.0)	70.8(1.3)	-0.51(0.22)	67.5(1.3)	1.19	3
70048-13-05-00	42106	52820.1519202	0.38	7.7(1.3)	496.97(0.86)	5.2(1.0)	59.6(1.3)	-0.71(0.22)	65.3(1.3)	1.21	3
70048-13-07-00	42413	52869.0685804	0.26	5.57(0.83)	491.94(0.52)	8.78(0.95)	90.4(1.6)	1.59(0.29)	99.6(1.6)	1.23	4
70048-13-08-00	42415	52869.3872676	0.33	7.92(0.93)	493.98(0.69)	5.05(0.72)	94.0(1.5)	0.28(0.25)	96.4(1.5)	1.24	4
70048-13-09-00	42416	52869.5466071	0.13	6.40(0.83)	495.31(0.49)	2.94(0.80)	89.8(1.6)	-0.41(0.29)	95.2(1.6)	1.18	4
70048-13-10-00	42417	52869.7059328	0.31	5.42(0.99)	492.72(0.69)	8.1(1.3)	67.3(1.3)	-0.38(0.23)	64.1(1.3)	1.27	3
80040-01-03-00	42618	52901.7328720	0.20	8.90(0.68)	499.57(0.69)	3.58(0.55)	104.3(1.7)	-0.95(0.31)	111.7(1.7)	1.12	4
80040-01-04-00	42632	52903.9635790	0.14	7.91(0.92)	495.23(0.49)	1.72(0.42)	88.7(1.1)	0.53(0.25)	85.0(1.1)	0.98	3
80040-01-04-01	42644	52905.8756264	0.36	8.2(1.0)	498.50(0.72)	8.76(0.97)	90.7(1.5)	-1.47(0.26)	93.2(1.6)	1.08	3
70048-13-11-00	42715	52917.1885901	0.35	9.2(1.1)	493.4(1.3)	5.41(0.90)	70.0(1.4)	-0.61(0.21)	65.1(1.3)	1.11	3
70048-13-12-00	42716	52917.3479105	0.22	5.23(0.67)	496.02(0.54)	4.56(0.79)	95.6(1.6)	0.67(0.25)	84.3(1.5)	1.18	4
70048-13-13-00	42717	52917.5072438	0.29	3.51(0.70)	494.21(0.74)	8.3(1.1)	70.3(1.5)	-1.09(0.30)	79.2(1.5)	1.19	3

Table 1—Continued

ObsID	Cycle Number	Mid-Eclipse Time (MJD;TDB)	Error (s)	Ingress Duration (s)	Totality Duration (s)	Egress Duration (s)	Pre-Ingress Count Rate (cnts s ⁻¹)	Totality Count Rate (cnts s ⁻¹)	Post-Egress Count Rate (cnts s ⁻¹)	Eclipse Fit χ_ν^2	Number of PCUs
70048-13-14-00	42718	52917.6665910	0.45	6.7(1.1)	495.2(1.0)	4.42(0.87)	55.8(1.2)	-0.78(0.21)	55.1(1.2)	1.08	2
70048-13-15-00	42719	52917.8259249	0.34	7.9(1.1)	493.02(0.91)	8.8(1.1)	72.3(1.4)	-0.82(0.23)	79.2(1.4)	1.34	3
80040-01-07-00	43065	52972.9567644	0.34	8.41(0.95)	504.87(0.84)	6.93(0.87)	121.7(1.8)	-0.96(0.31)	111.2(1.7)	1.30	4
70048-13-16-00	43095	52977.7369723	0.42	29.7(1.9)	490.2(1.0)	4.1(1.0)	101.0(1.6)	1.21(0.27)	48.4(1.2)	1.33	4
70048-13-17-00	43096	52977.8962834	0.58	30.7(2.2)	488.0(1.3)	9.6(1.7)	74.4(1.1)	0.00(0.25)	56.15(0.91)	1.37	3
70048-13-18-00	43097	52978.0556884	0.32	35.3(2.3)	492.23(0.98)	4.11(0.87)	81.0(1.1)	0.61(0.25)	69.87(0.99)	1.31	3
70048-13-19-00G	43098	52978.2148911	0.37	9.7(1.5)	501.02(0.86)	4.1(1.2)	53.5(1.2)	-1.39(0.19)	30.9(1.0)	1.34	2
70048-13-20-00	43099	52978.3743057	0.20	28.4(1.9)	491.0(1.1)	1.89(0.64)	98.2(1.2)	1.35(0.27)	80.8(1.0)	1.38	4
80040-01-06-00	43342	53017.0933503	0.25	7.00(0.79)	493.52(0.91)	8.39(0.87)	103.6(1.6)	-1.26(0.26)	105.6(1.6)	1.12	3
90059-01-01-00	43414	53028.5657012	0.24	6.96(0.72)	500.12(0.50)	5.31(0.65)	118.1(1.7)	0.31(0.26)	119.7(1.7)	1.19	4
90059-01-02-00	43415	53028.7250264	0.19	6.03(0.54)	495.64(0.41)	9.99(0.63)	119.8(1.7)	-0.56(0.24)	125.9(1.7)	1.17	4
90059-01-03-00	43416	53028.8843749	0.20	7.04(0.75)	498.50(0.45)	5.52(0.66)	119.0(1.7)	-0.06(0.25)	124.6(1.7)	1.22	4
90059-01-04-00	43417	53029.0437272	0.13	3.50(0.40)	500.09(0.34)	2.22(0.34)	92.1(1.5)	-1.24(0.20)	91.1(1.5)	1.10	3
90059-02-01-00	43684	53071.5869069	0.069	1.07(0.16)	491.10(0.22)	3.71(0.55)	116.2(1.7)	-0.84(0.24)	116.2(1.7)	1.02	4
90059-02-02-00	43685	53071.7462444	0.19	3.14(0.57)	489.80(0.43)	3.45(0.55)	85.4(1.4)	-1.05(0.20)	88.7(1.5)	1.03	3
90059-02-03-00	43686	53071.9055841	0.037	2.11(0.45)	491.02(0.18)	2.95(0.59)	112.2(1.6)	-1.11(0.21)	111.8(1.6)	1.10	3
90059-02-04-00	43687	53072.0649216	0.10	1.04(0.34)	491.75(0.23)	1.66(0.25)	111.8(1.6)	-0.44(0.20)	103.4(1.6)	1.04	3
80040-01-10-01	43998	53121.6189689	0.11	6.98(0.55)	489.49(0.34)	2.42(0.32)	160.7(2.0)	-1.70(0.29)	167.9(2.0)	1.00	4
90059-03-01-00	44028	53126.3991026	0.16	3.58(0.36)	490.68(0.33)	3.28(0.34)	137.5(1.8)	-1.10(0.23)	130.6(1.8)	1.03	4
90059-03-02-00	44029	53126.5584450	0.15	5.11(0.48)	488.75(0.30)	4.44(0.54)	121.2(1.7)	-1.18(0.23)	121.7(1.7)	1.05	4
90059-03-03-00	44030	53126.7177783	0.21	6.23(0.74)	489.31(0.60)	4.48(0.69)	87.6(1.4)	-1.02(0.20)	83.4(1.4)	1.03	3
90059-03-04-00	44031	53126.8771141	0.17	5.59(0.65)	489.67(0.39)	4.19(0.49)	93.2(1.5)	-1.12(0.20)	94.0(1.5)	1.03	3
80040-01-11-00G	44319	53172.7663908	0.15	3.93(0.46)	490.06(0.36)	7.59(0.54)	108.0(1.7)	-2.26(0.25)	110.0(1.7)	1.03	3
80040-01-11-00G	44320	53172.9257310	0.14	4.27(0.53)	489.31(0.30)	2.05(0.28)	107.7(1.7)	-2.36(0.25)	115.9(1.7)	1.07	3
90059-04-04-00	44360	53179.2992475	0.15	8.21(0.62)	488.45(0.40)	3.78(0.53)	133.7(1.8)	-0.12(0.22)	134.3(1.7)	1.09	3
90059-04-03-00	44361	53179.4585790	0.11	1.92(0.28)	490.54(0.20)	1.88(0.47)	137.2(1.8)	-1.05(0.21)	130.7(1.7)	1.03	3
90059-04-02-00	44362	53179.6179183	0.11	6.04(0.46)	489.92(0.23)	3.43(0.39)	131.7(1.7)	-0.75(0.22)	120.9(1.7)	1.21	3
90059-04-01-00	44363	53179.7772562	0.11	9.86(0.64)	489.62(0.31)	3.04(0.37)	148.1(1.8)	-0.72(0.22)	140.5(1.8)	1.16	3
80040-01-12-07	44620	53220.7270511	0.31	2.91(0.86)	489.73(0.72)	4.6(1.2)	55.51(0.97)	-2.02(0.25)	56.93(0.97)	1.02	3
90059-05-01-00	44673	53229.1719648	0.19	3.27(0.95)	489.41(0.43)	2.29(0.56)	48.1(1.2)	-2.13(0.21)	48.1(1.2)	1.06	3
90059-05-02-00	44674	53229.3312967	0.29	2.65(0.83)	489.08(0.70)	3.8(1.1)	46.2(1.1)	-2.67(0.22)	46.4(1.1)	1.24	3
90059-05-03-00	44675	53229.4906415	0.17	2.91(0.66)	490.24(0.38)	2.69(0.58)	49.7(1.2)	-1.79(0.20)	50.1(1.2)	1.10	3

Table 1—Continued

ObsID	Cycle Number	Mid-Eclipse Time (MJD;TDB)	Error (s)	Ingress Duration (s)	Totality Duration (s)	Egress Duration (s)	Pre-Ingress Count Rate (cnts s ⁻¹)	Totality Count Rate (cnts s ⁻¹)	Post-Egress Count Rate (cnts s ⁻¹)	Eclipse Fit χ_ν^2	Number of PCUs
90059-05-04-00	44676	53229.6499829	0.31	4.11(0.90)	489.54(0.92)	2.84(0.77)	30.85(0.95)	-2.07(0.17)	31.97(0.95)	1.11	2
90059-06-01-00	44949	53273.1491878	0.25	9.21(0.77)	493.63(0.53)	7.12(0.79)	119.1(1.7)	-1.74(0.24)	99.7(1.6)	1.15	4
90059-06-02-00	44950	53273.3085110	0.31	4.73(0.89)	490.79(0.70)	5.6(1.0)	47.1(1.1)	-2.42(0.19)	48.7(1.1)	1.24	2
90059-06-03-00	44951	53273.4678599	0.089	5.27(0.92)	493.09(0.47)	0.78(0.28)	66.2(1.3)	-1.89(0.21)	66.3(1.3)	1.12	3
90059-06-04-00	44952	53273.6272033	0.31	8.26(0.81)	491.07(0.65)	5.39(0.72)	65.0(1.3)	-1.47(0.20)	65.9(1.3)	1.07	3
80040-01-13-01	44972	53276.8139438	0.13	3.59(0.45)	495.52(0.33)	1.49(0.40)	78.8(1.5)	-2.67(0.25)	81.4(1.5)	1.12	3
80040-01-13-02	44979	53277.9293193	0.21	9.86(0.80)	489.87(0.74)	3.72(0.58)	82.7(1.5)	-2.11(0.27)	73.7(1.5)	1.13	3
90039-01-02-00	45261	53322.8625796	0.085	3.89(0.34)	490.82(0.20)	2.32(0.25)	205.9(2.2)	-1.00(0.30)	211.4(2.3)	0.99	4
90039-01-03-01	45310	53330.6701347	0.21	8.22(0.63)	489.90(0.56)	1.93(0.41)	96.8(1.6)	-3.02(0.28)	93.9(1.6)	1.01	4
90059-07-01-00	45318	53331.9448389	0.18	3.22(0.51)	493.14(0.45)	3.62(0.67)	81.5(1.4)	-2.01(0.23)	82.1(1.5)	1.10	4
90059-07-02-00	45319	53332.1041790	0.18	9.37(0.79)	489.51(0.61)	1.68(0.58)	62.5(1.3)	-1.71(0.21)	63.5(1.3)	1.11	3
90059-07-03-00	45320	53332.2635053	0.19	4.21(0.71)	490.94(0.39)	2.44(0.53)	87.0(1.5)	-1.29(0.23)	89.2(1.5)	1.06	4
90059-07-04-00	45321	53332.4228631	0.078	5.79(0.84)	495.72(0.42)	0.74(0.24)	66.9(1.3)	-1.94(0.20)	66.1(1.3)	1.10	3
90059-08-04-00	45606	53377.8341065	0.16	5.28(0.52)	491.34(0.32)	4.42(0.54)	123.2(1.7)	-0.30(0.25)	124.1(1.7)	1.14	4
90059-08-03-00	45607	53377.9934542	0.16	10.37(0.74)	490.94(0.50)	3.15(0.52)	136.7(1.8)	-0.33(0.25)	137.5(1.8)	1.16	4
90059-08-02-00	45609	53378.3121347	0.18	8.83(0.61)	493.37(0.43)	3.43(0.47)	106.1(1.6)	-0.66(0.21)	96.5(1.5)	1.09	3
90059-09-01-00	45943	53431.5309277	0.22	7.55(0.83)	494.09(0.53)	8.23(0.78)	100.0(1.6)	-0.66(0.22)	101.3(1.6)	1.13	3
90059-09-02-00	45944	53431.6902678	0.27	5.58(0.68)	497.86(0.53)	5.96(0.75)	102.3(1.5)	-0.29(0.21)	102.8(1.6)	1.16	3
90059-09-03-00	45945	53431.8496134	0.094	9.19(0.90)	496.64(0.52)	1.07(0.38)	101.7(1.6)	-0.21(0.22)	98.1(1.5)	1.15	3
90059-09-04-00	45947	53432.1682753	0.16	7.48(0.58)	494.70(0.33)	5.25(0.46)	167.4(2.0)	0.97(0.29)	169.2(2.0)	1.16	5
91043-01-01-00	46250	53480.4476510	0.088	10.40(0.55)	493.43(0.25)	1.97(0.26)	276.6(2.4)	6.26(0.29)	262.0(2.4)	1.23	4
91043-01-02-00	46251	53480.6069891	0.11	8.40(0.39)	494.98(0.24)	5.24(0.37)	252.4(2.3)	4.29(0.25)	235.4(2.3)	1.24	3
91043-01-03-00	46252	53480.7663246	0.12	9.53(0.54)	494.12(0.30)	5.13(0.32)	257.9(2.3)	4.55(0.26)	266.8(2.4)	1.27	3
91043-01-04-00	46253	53480.9256602	0.11	8.83(0.51)	493.51(0.25)	4.46(0.35)	243.4(2.3)	5.00(0.24)	239.6(2.3)	1.12	3
91035-01-02-06	46285	53486.0244603	0.13	6.93(0.51)	493.05(0.27)	4.29(0.39)	206.2(2.2)	2.16(0.30)	198.0(2.1)	1.14	3
91035-01-03-04	46294	53487.4585112	0.12	8.52(0.55)	492.49(0.30)	2.74(0.37)	203.4(2.1)	1.31(0.27)	195.1(2.1)	1.09	3
91035-01-03-07	46301	53488.5738684	0.096	6.78(0.51)	493.06(0.24)	2.78(0.28)	210.9(2.2)	2.06(0.26)	211.6(2.2)	1.02	3
91043-02-01-00	46582	53533.3477768	0.21	7.67(0.84)	496.82(0.45)	2.67(0.59)	83.2(1.5)	-1.26(0.22)	86.6(1.5)	1.12	3
91043-02-02-00	46583	53533.5071052	0.30	9.6(1.0)	493.07(0.62)	6.35(0.88)	84.1(1.4)	-1.59(0.22)	82.5(1.4)	1.16	3
91043-02-03-00	46584	53533.6664512	0.32	9.53(0.90)	493.97(0.72)	4.31(0.71)	58.2(1.2)	-1.68(0.20)	56.6(1.2)	1.20	2
91043-02-04-00	46587	53534.1444468	0.24	9.3(1.2)	498.24(0.89)	2.80(0.60)	56.4(1.2)	-1.49(0.18)	55.0(1.2)	1.10	2
91043-03-03-00	46878	53580.5118166	0.10	8.81(0.73)	494.41(0.47)	1.34(0.28)	139.4(1.9)	0.34(0.26)	137.0(1.8)	1.15	4

Table 1—Continued

ObsID	Cycle Number	Mid-Eclipse Time (MJD;TDB)	Error (s)	Ingress Duration (s)	Totality Duration (s)	Egress Duration (s)	Pre-Ingress Count Rate (cnts s ⁻¹)	Totality Count Rate (cnts s ⁻¹)	Post-Egress Count Rate (cnts s ⁻¹)	Eclipse Fit χ_ν^2	Number of PCUs
91043-03-04-00	46879	53580.6711422	0.28	9.22(0.81)	491.61(0.50)	5.92(0.71)	99.2(1.6)	-0.77(0.23)	101.1(1.6)	1.06	3
91043-03-01-00	46881	53580.9898127	0.22	11.23(0.95)	489.65(0.50)	5.13(0.55)	92.6(1.5)	-1.39(0.20)	97.1(1.5)	1.07	3
91043-03-02-00	46882	53581.1491684	0.17	9.74(0.73)	490.33(0.37)	5.17(0.57)	147.9(1.8)	-0.92(0.24)	147.5(1.9)	1.12	4
91043-04-01-00	47183	53629.1098320	0.26	12.0(1.4)	494.34(0.57)	4.65(0.86)	65.0(1.3)	-0.95(0.21)	68.2(1.3)	1.12	3
91043-04-02-00	47184	53629.2691584	0.36	12.7(1.6)	492.85(0.85)	6.7(1.1)	45.4(1.1)	-1.29(0.19)	47.2(1.1)	1.17	2
91043-04-03-00	47185	53629.4284882	0.29	7.8(1.3)	494.96(0.87)	1.85(0.59)	45.2(1.1)	-1.26(0.18)	45.3(1.1)	1.10	2
91043-04-04-00	47186	53629.5878297	0.19	5.81(0.84)	498.04(0.59)	3.73(0.70)	43.5(1.1)	-1.65(0.18)	44.1(1.1)	1.17	2
91043-05-01-00	47523	53683.2846661	0.33	11.0(1.1)	492.99(0.67)	6.98(0.91)	89.4(1.5)	-1.03(0.22)	88.9(1.5)	1.24	3
91043-05-02-00	47524	53683.4440071	0.38	11.2(1.4)	491.9(1.0)	8.9(1.2)	62.5(1.2)	-1.05(0.19)	61.9(1.3)	1.22	2
91043-05-03-00	47525	53683.6033538	0.22	9.82(0.75)	494.59(0.48)	5.43(0.64)	89.0(1.5)	-1.11(0.22)	90.1(1.5)	1.25	3
91043-05-04-00	47526	53683.7627048	0.10	15.4(1.2)	491.09(0.65)	2.56(0.34)	113.9(1.7)	0.03(0.25)	115.0(1.6)	1.21	4
91043-06-01-00 ^a	47889	53741.6023456	0.16	3.93(0.56)	491.34(0.84)	2.79(0.54)	78.4(1.4)	-0.50(0.22)	85.0(1.5)	1.08	3
91043-06-01-01 ^a	47890	53741.7616499	0.19	8.37(0.68)	496.70(0.39)	3.89(0.51)	141.4(1.8)	-0.55(0.25)	117.0(1.7)	1.12	4
91043-06-02-00 ^a	47891	53741.9209836	0.19	4.16(0.53)	499.97(0.39)	6.27(0.54)	111.6(1.6)	-0.85(0.24)	111.3(1.7)	1.13	4
91043-06-03-00 ^a	47892	53742.0803292	0.21	7.22(0.74)	497.88(0.42)	4.25(0.60)	87.7(1.5)	-1.08(0.21)	84.2(1.5)	1.10	3
91043-06-04-00 ^a	47893	53742.2396852	0.30	9.50(0.89)	499.50(0.62)	7.30(0.74)	105.7(1.6)	-1.77(0.23)	102.8(1.6)	1.13	4
91043-07-01-00	48155	53783.9861861	0.12	1.87(0.58)	499.50(0.32)	3.00(0.86)	36.2(1.0)	-1.60(0.18)	34.7(1.0)	1.09	2
91043-07-02-00	48156	53784.1455430	0.34	6.8(1.4)	492.5(1.0)	1.53(0.70)	36.7(1.0)	-1.97(0.17)	36.4(1.0)	1.12	2
91043-07-03-00	48157	53784.3048515	0.12	4.3(1.0)	497.60(0.46)	0.75(0.35)	37.2(1.0)	-1.76(0.17)	36.9(1.0)	1.12	2
91043-07-04-00	48158	53784.4642033	0.35	6.7(1.2)	497.29(0.90)	7.9(1.6)	36.7(1.0)	-2.32(0.18)	36.6(1.0)	1.11	2
90059-10-01-00	48472	53834.4963316	0.23	7.2(1.0)	498.31(0.69)	6.4(1.0)	72.0(1.4)	-1.35(0.22)	72.6(1.4)	1.13	3
90059-10-02-00	48473	53834.6556389	0.22	6.28(0.69)	500.65(0.42)	4.22(0.58)	97.3(1.6)	-1.10(0.23)	97.7(1.6)	1.08	4
90059-10-03-00	48474	53834.8149977	0.19	4.67(0.96)	496.82(0.70)	1.93(0.93)	47.6(1.1)	-1.31(0.17)	48.7(1.1)	1.02	2
90059-10-04-00	48475	53834.9743398	0.25	1.24(0.38)	494.29(0.42)	3.57(0.77)	49.6(1.1)	-1.41(0.17)	50.3(1.1)	1.06	2
90059-11-01-00	48791	53885.3250824	0.30	7.90(0.97)	496.01(0.79)	8.43(0.95)	77.4(1.4)	-1.81(0.22)	79.4(1.4)	1.08	3
90059-11-02-00	48792	53885.4844268	0.20	5.19(0.73)	497.08(0.46)	3.41(0.63)	78.2(1.4)	-1.70(0.21)	76.3(1.4)	1.17	3
90059-11-03-00	48795	53885.9624781	0.22	7.11(0.91)	502.84(0.50)	5.62(0.82)	67.9(1.4)	-1.59(0.22)	71.7(1.3)	1.11	3
90059-11-04-00	48796	53886.1218228	0.086	3.97(0.84)	502.00(0.20)	4.28(0.85)	69.5(1.3)	-1.54(0.21)	68.7(1.3)	1.07	3
90059-12-01-00	49082	53931.6924423	0.20	3.09(0.63)	500.40(0.40)	4.66(0.79)	57.4(1.3)	-1.50(0.21)	58.0(1.3)	1.17	3
90059-12-02-00	49083	53931.8517613	0.34	6.25(0.95)	499.38(0.71)	7.4(1.1)	58.3(1.3)	-2.12(0.21)	57.4(1.3)	1.21	3
90059-12-03-00	49084	53932.0111217	0.32	7.74(0.92)	498.49(0.67)	5.18(0.78)	56.8(1.3)	-1.09(0.22)	58.1(1.3)	1.15	3
90059-12-04-00	49085	53932.1704326	0.57	4.8(2.3)	500.8(1.4)	7.6(1.9)	18.80(0.51)	-1.31(0.11)	18.57(0.51)	1.36	1

Table 1—Continued

ObsID	Cycle Number	Mid-Eclipse Time (MJD;TDB)	Error (s)	Ingress Duration (s)	Totality Duration (s)	Egress Duration (s)	Pre-Ingress Count Rate (cnts s ⁻¹)	Totality Count Rate (cnts s ⁻¹)	Post-Egress Count Rate (cnts s ⁻¹)	Eclipse Fit χ_ν^2	Number of PCUs
92019-01-01-00	49396	53981.7244969	0.44	5.7(1.0)	496.11(0.95)	6.8(1.1)	37.9(1.1)	-2.58(0.20)	38.9(1.1)	1.04	2
91043-08-01-00	49424	53986.1859569	0.19	3.68(0.70)	497.29(0.41)	2.89(0.66)	53.3(1.2)	-1.93(0.21)	54.3(1.2)	1.07	3
91043-08-02-00	49425	53986.3453084	0.28	9.0(1.2)	493.66(0.85)	2.76(0.95)	35.8(1.0)	-2.45(0.18)	34.6(1.0)	1.11	2
91043-08-03-00	49426	53986.5046257	0.29	4.79(0.83)	498.58(0.83)	1.94(0.68)	36.7(1.0)	-2.38(0.18)	36.6(1.0)	1.16	2
91043-08-04-00	49427	53986.6639612	0.24	2.04(0.61)	495.89(0.60)	5.5(1.0)	55.5(1.2)	-2.23(0.21)	55.5(1.2)	1.13	3
92019-01-04-01	49440	53988.7353550	0.18	3.59(0.70)	499.39(0.44)	4.25(0.81)	57.5(1.3)	-2.51(0.25)	57.2(1.3)	1.03	3
92019-01-04-03	49447	53989.8507114	0.42	2.69(0.97)	499.46(0.76)	4.6(1.1)	37.2(1.0)	-2.59(0.18)	38.0(1.0)	1.10	2
92019-01-03-000	49452	53990.6474142	0.27	4.58(0.83)	494.69(0.59)	6.61(0.87)	64.3(1.4)	-2.79(0.28)	65.5(1.4)	1.14	3
92019-01-03-00	49454	53990.9660841	0.39	8.1(1.2)	496.13(0.79)	6.8(1.1)	64.0(1.4)	-2.41(0.25)	65.4(1.4)	1.00	3
92019-01-01-04	49470	53993.5154954	0.21	5.91(0.96)	497.78(0.69)	4.09(0.86)	40.3(1.1)	-2.61(0.20)	41.1(1.1)	1.11	2
92019-01-05-00	49477	53994.6308650	0.41	8.5(1.5)	494.6(1.1)	4.9(1.1)	43.7(1.2)	-2.12(0.22)	43.4(1.2)	1.06	2
92019-01-06-02	49560	54007.8558626	0.36	6.6(1.1)	490.19(0.87)	4.8(1.0)	56.9(1.3)	-3.07(0.23)	54.3(1.2)	1.39	2
92019-01-08-000	49717	54032.8719384	0.21	3.89(0.53)	498.73(0.54)	8.22(0.63)	104.2(1.7)	-2.20(0.27)	101.5(1.6)	1.18	3
92019-01-08-000	49718	54033.0312724	0.37	11.1(1.2)	495.45(0.81)	9.5(1.3)	62.3(1.3)	-2.47(0.20)	62.7(1.3)	1.16	2
91043-09-01-00	49724	54033.9873060	0.20	6.35(0.76)	501.10(0.52)	3.55(0.64)	89.4(1.5)	-0.80(0.23)	87.7(1.5)	1.14	3
91043-09-02-00	49725	54034.1466424	0.16	8.2(1.0)	500.27(0.53)	5.22(0.88)	87.2(1.5)	-1.52(0.23)	90.1(1.5)	1.32	3
91043-09-04-00	49726	54034.3059939	0.27	8.46(0.92)	497.74(0.57)	5.24(0.78)	88.8(1.5)	-1.14(0.21)	89.4(1.5)	1.17	3
91043-09-03-00	49727	54034.4653135	0.18	2.25(0.40)	501.66(0.35)	5.25(0.78)	90.5(1.5)	-1.09(0.21)	90.8(1.5)	1.20	3
91043-10-01-00	50032	54083.0633645	0.088	5.45(0.43)	497.96(0.21)	2.92(0.30)	237.6(2.3)	2.92(0.24)	230.1(2.2)	1.22	3
91043-10-02-00	50033	54083.2226981	0.13	10.95(0.50)	498.58(0.34)	5.10(0.40)	174.4(2.0)	1.77(0.20)	173.0(1.9)	1.14	2
91043-10-03-00	50034	54083.3820350	0.12	5.77(0.38)	498.38(0.24)	3.95(0.32)	229.7(2.2)	3.66(0.25)	223.4(2.2)	1.28	3
91043-10-04-00	50035	54083.5413725	0.20	7.2(1.0)	497.65(0.47)	3.07(0.64)	60.13(0.83)	0.69(0.12)	60.48(0.83)	1.07	1
91043-12-01-00	50094	54092.9422986	0.088	5.95(0.32)	497.51(0.26)	3.24(0.26)	243.8(2.2)	3.61(0.25)	238.0(2.3)	1.20	3
91043-12-02-00	50095	54093.1016406	0.086	4.45(0.33)	495.78(0.17)	4.57(0.37)	246.1(2.3)	2.94(0.24)	239.5(2.3)	1.21	3
91043-12-03-00	50096	54093.2609694	0.12	5.25(0.52)	495.03(0.26)	6.38(0.58)	155.4(1.8)	0.65(0.17)	148.1(1.8)	1.36	2
91043-12-04-01	50097	54093.4203145	0.11	7.44(0.41)	496.54(0.25)	3.19(0.34)	206.6(2.1)	1.67(0.21)	208.5(2.1)	1.24	3
91043-12-04-00	50098	54093.5796468	0.096	3.88(0.34)	496.44(0.20)	3.93(0.32)	258.4(2.4)	3.00(0.26)	277.5(2.5)	1.13	4
91043-11-01-00	50375	54137.7162276	0.42	4.4(1.1)	491.56(0.92)	7.7(1.4)	42.7(1.1)	-1.37(0.21)	43.2(1.1)	1.11	3
91043-11-01-01	50376	54137.8755569	0.88	5.8(1.3)	492.8(1.6)	7.8(1.5)	50.0(1.2)	2.09(0.23)	49.4(1.2)	1.04	3
91043-11-02-00	50377	54138.0349017	0.28	5.0(1.5)	493.84(0.81)	3.1(1.1)	31.83(0.95)	1.75(0.18)	31.95(0.92)	1.10	2
91043-11-03-00	50378	54138.1942388	0.36	8.1(1.2)	492.9(1.3)	5.7(1.2)	34.14(0.96)	1.63(0.17)	33.82(0.96)	1.05	2
91043-11-04-00	50379	54138.3535786	0.33	8.5(1.6)	490.32(0.69)	6.1(1.3)	47.4(1.2)	0.68(0.23)	49.7(1.2)	1.12	3

Table 1—Continued

ObsID	Cycle Number	Mid-Eclipse Time (MJD;TDB)	Error (s)	Ingress Duration (s)	Totality Duration (s)	Egress Duration (s)	Pre-Ingress Count Rate (cnts s ⁻¹)	Totality Count Rate (cnts s ⁻¹)	Post-Egress Count Rate (cnts s ⁻¹)	Eclipse Fit χ_ν^2	Number of PCUs
92040-01-01-00	50672	54185.0395258	0.40	4.35(0.90)	486.80(0.86)	9.3(1.2)	46.5(1.2)	-1.63(0.22)	46.0(1.2)	1.17	3
92040-01-02-00	50673	54185.1989149	0.38	7.6(1.2)	493.25(0.83)	5.5(1.1)	66.6(1.4)	1.84(0.25)	63.4(1.3)	1.07	4
92040-01-03-00	50674	54185.3582214	0.51	5.75(0.92)	489.6(1.1)	12.3(1.2)	66.7(1.4)	1.99(0.26)	63.2(1.3)	1.19	4
92040-01-04-00	50675	54185.5174975	0.44	3.57(0.98)	486.3(1.5)	17.3(1.7)	32.14(0.71)	-0.07(0.19)	32.60(0.75)	1.05	2
92040-02-01-00	51013	54239.3737259	0.20	1.48(0.40)	490.4(1.1)	23.6(1.9)	59.62(0.89)	0.33(0.19)	60.80(0.96)	1.05	2
92040-02-02-00	51014	54239.5330818	0.23	3.50(0.67)	493.53(0.84)	14.8(1.3)	60.25(0.88)	1.79(0.21)	78.5(1.0)	1.24	2
92040-02-03-00	51015	54239.6924005	0.27	4.90(0.83)	489.99(0.81)	22.4(1.7)	63.09(0.91)	0.43(0.19)	63.51(0.97)	1.04	2
92040-02-04-00	51016	54239.8517268	0.31	5.98(0.99)	491.50(0.97)	24.0(1.9)	72.58(0.95)	3.61(0.20)	68.42(0.99)	1.28	2
93074-01-01-00	51308	54286.3784178	0.32	9.52(0.95)	493.87(0.94)	7.47(0.87)	65.5(1.3)	-1.76(0.20)	65.6(1.3)	1.22	2
93074-01-02-00	51309	54286.5377532	0.20	2.85(0.58)	493.73(0.46)	8.1(1.1)	66.1(1.3)	-1.07(0.19)	63.3(1.3)	1.18	2
93074-01-03-00	51310	54286.6970901	0.22	6.56(0.93)	498.82(0.47)	6.83(0.92)	62.5(1.3)	-1.17(0.19)	63.2(1.3)	1.18	2
93074-01-04-00	51311	54286.8564419	0.26	4.15(0.67)	494.14(0.58)	8.39(0.97)	67.3(1.2)	2.03(0.18)	67.9(1.3)	1.12	2
93074-02-01-00	51658	54342.1466707	0.16	6.27(0.76)	497.06(0.41)	3.39(0.60)	78.2(1.4)	0.11(0.22)	87.0(1.5)	1.12	3
93074-02-03-00	51659	54342.3059952	0.34	7.12(0.86)	491.41(0.71)	6.92(0.93)	85.4(1.5)	-0.16(0.22)	85.2(1.5)	1.03	3
93074-02-04-00	51661	54342.6246716	0.31	7.32(0.75)	498.03(0.67)	5.15(0.69)	86.0(1.4)	2.98(0.19)	68.0(1.3)	1.20	2
93074-03-01-00	51953	54389.1513218	0.41	5.89(0.82)	492.95(0.65)	7.07(0.97)	89.2(1.5)	2.69(0.25)	91.0(1.5)	1.22	3
93074-03-03-00	51955	54389.4699771	0.25	10.33(0.91)	495.91(0.59)	3.56(0.70)	61.6(1.3)	-0.91(0.20)	57.7(1.2)	1.16	2
93074-03-04-00	51956	54389.6293267	0.35	7.0(1.2)	493.51(0.73)	5.6(1.0)	31.36(0.97)	-1.63(0.16)	39.5(1.1)	1.22	2
93074-04-01-01	52266	54439.0240582	0.15	1.69(0.41)	495.15(0.55)	6.15(0.99)	55.6(1.2)	-0.99(0.18)	58.8(1.2)	1.07	2
93074-04-01-00	52267	54439.1833808	0.29	3.98(0.75)	492.51(0.64)	7.02(0.95)	50.18(0.83)	-0.17(0.20)	54.66(0.87)	1.06	2
93074-04-02-00	52268	54439.3427276	0.28	5.8(1.2)	491.02(0.96)	5.6(1.2)	54.3(1.2)	-1.82(0.21)	44.8(1.1)	1.31	2
93074-04-03-00	52269	54439.5020647	0.28	7.9(1.7)	489.4(1.2)	2.63(0.81)	22.80(0.55)	-1.11(0.11)	22.75(0.55)	1.15	1
93074-04-04-00	52270	54439.6614473	0.32	9.3(1.7)	494.58(0.92)	2.90(0.95)	22.26(0.54)	-0.92(0.10)	22.08(0.54)	1.17	1
93074-05-01-01	52615	54494.6329444	0.21	2.72(0.53)	489.04(0.57)	5.44(0.67)	67.3(1.4)	-1.31(0.23)	67.0(1.3)	1.22	3
93074-05-01-00	52616	54494.7922908	0.095	2.5(1.1)	492.03(0.31)	3.3(1.2)	43.6(1.1)	-1.80(0.19)	42.5(1.1)	1.24	2
93074-05-02-00	52617	54494.9516528	0.18	6.42(0.85)	494.64(0.61)	2.79(0.63)	37.4(1.0)	-2.26(0.15)	38.5(1.0)	1.32	2
93074-05-03-00	52618	54495.1110034	0.46	5.5(1.1)	493.8(1.1)	2.1(1.1)	18.47(0.50)	-0.93(0.11)	16.25(0.47)	1.26	1
93074-05-04-00	52619	54495.2702930	0.58	8.8(2.1)	485.5(1.4)	11.4(2.8)	19.59(0.52)	-1.15(0.11)	19.25(0.52)	1.37	1
93074-05-04-01	52620	54495.4296653	0.23	8.0(1.1)	494.40(0.44)	3.74(0.75)	61.4(1.2)	0.25(0.23)	58.6(1.3)	1.17	3
93074-06-01-00	52928	54544.5056972	0.18	1.86(0.54)	502.71(0.40)	3.62(0.66)	51.0(1.2)	-0.45(0.17)	54.0(1.2)	1.22	2
93074-06-02-00	52929	54544.6650528	0.28	5.9(1.1)	501.19(0.73)	3.18(0.70)	46.6(1.1)	-1.73(0.16)	49.0(1.1)	1.44	2
93074-06-03-00	52930	54544.8243556	0.11	0.87(0.41)	501.58(0.61)	7.7(1.3)	49.7(1.1)	-2.07(0.15)	49.1(1.1)	1.41	2

Table 1—Continued

ObsID	Cycle Number	Mid-Eclipse Time (MJD;TDB)	Error (s)	Ingress Duration (s)	Totality Duration (s)	Egress Duration (s)	Pre-Ingress Count Rate (cnts s ⁻¹)	Totality Count Rate (cnts s ⁻¹)	Post-Egress Count Rate (cnts s ⁻¹)	Eclipse Fit χ_ν^2	Number of PCUs
93074-06-04-01	52932	54545.1430711	0.23	7.3(1.5)	498.85(0.83)	4.2(1.6)	26.38(0.58)	-0.73(0.11)	26.85(0.58)	1.40	1
92040-03-01-00	53284	54601.2299407	0.19	1.69(0.45)	501.73(0.52)	4.72(0.82)	59.1(1.2)	2.42(0.19)	57.5(1.2)	1.09	2
92040-03-02-00	53285	54601.3892854	0.26	4.91(0.76)	498.66(0.56)	6.32(0.82)	56.2(1.2)	1.46(0.19)	57.0(1.2)	1.24	2
92040-03-03-00	53286	54601.5486082	0.37	2.32(0.57)	499.02(0.71)	7.6(1.1)	55.6(1.2)	-1.43(0.18)	57.0(1.2)	1.10	2
92040-03-04-00	53287	54601.7079405	0.38	9.83(0.97)	490.6(1.0)	8.00(0.95)	50.6(1.1)	-2.32(0.14)	50.7(1.1)	1.19	2
92040-04-01-00	53567	54646.3225178	0.31	3.40(0.72)	498.01(0.93)	3.35(0.64)	41.8(1.1)	-1.66(0.19)	49.5(1.2)	1.05	2
92040-04-02-00	53568	54646.4818452	0.39	11.8(1.5)	494.61(0.91)	8.7(1.6)	42.6(1.0)	2.08(0.18)	43.2(1.6)	1.06	2
92040-04-04-00	53570	54646.8005347	0.36	8.2(1.5)	492.36(0.75)	5.3(1.2)	41.9(1.0)	1.77(0.18)	42.4(1.0)	1.08	2

^aOn January 16, 2009, the RXTE Guest Observer Facility announced that a one-second timing error had been discovered in the raw data files from observations in the date range 1-12 January, 2006. The fitted mid-eclipse time for this ObsID has been corrected for this error. Information regarding this error can be found at the web address http://heasarc.gsfc.nasa.gov/docs/xte/xhp_new.html#timingerror

Table 2. Unusable Observed EXO 0748–676 Eclipses

ObsID	Cycle	Comment
10108-01-10-00	26357	Eclipse unusable; PCU4 switch-on with bad EDS mode.
20069-01-04-00	27003	Missing GoodXenon data file.
20069-05-05-00	28335	X-Ray burst during totality with decay after egress.
20082-01-03-05	28688	Ingress only in data.
20082-01-03-00	28691	Ingress only in data.
30067-04-03-00	30999	X-Ray burst during ingress; Eclipse profile corrupted.
40039-01-03-00	31958	Egress profile hidden by data gap.
40039-04-05-00	32969	X-ray burst before ingress distorts profile.
40039-05-01-00	33265	Ingress only in data.
40039-06-01-00	33621	X-Ray Burst during totality with decay after egress.
40039-06-05-00G	33626	Data gap covers entire eclipse.
50045-01-04-00	34651	X-Ray burst during totality, decay after egress.
50045-03-02-00	35305	X-ray burst before ingress distorts profile.
50045-03-05-00G	35309	X-ray burst before ingress distorts profile.
50045-06-02-00	36306	X-Ray burst right at egress makes eclipse unusable.
50045-06-05-00	36310	X-Ray burst during totality with decay after egress.
70048-02-04-00	39162	Double X-ray burst distorts eclipse.
70048-06-03-00	40010	Data dropout at egress.
70048-07-04-00	40213	Source too close to earth limb: Light Curve distorted.
60042-03-01-03	40799	Egress only in data.
60042-03-02-03	40818	Egress only in data.
60042-03-02-02	40825	Egress only in data.
60042-03-02-00	40837	Egress only in data.
70047-01-01-03	41252	Egress only in data.
70047-01-01-06	41253	Egress only in data.
70047-01-01-07	41254	Ingress only in data.
70047-02-01-10	41283	Ingress only in data.
70048-13-03-00	42103	Data dropout too close to ingress.
80040-01-01-01	42112	Egress only in data.
70048-13-06-00	42412	X-Ray burst during totality with decay after egress.

Table 2—Continued

ObsID	Cycle	Comment
80040-01-03-00	42619	Egress only in data.
80040-01-06-07	43489	Egress only in data.
80040-01-09-00	43748	Ingress only in data.
90039-01-01-00	45235	Egress only in data.
90039-01-02-08	45289	Egress only in data.
90039-01-03-00	45298	Egress only in data.
90039-01-03-05	45335	Egress only in data.
90039-01-03-05	45336	Ingress only in data.
90059-08-01-00	45608	Electron event during totality distorts flux level.
91035-01-01-07	46264	Ingress only in data.
91035-01-04-12	46338	Egress only in data.
92019-01-01-00	49395	Egress only in data.
92019-01-07-00	49692	Ingress only in data.
93074-02-02-00	51660	Data dropout during ingress makes eclipse unusable.
93074-03-02-00	51953	Egress only in data.
93074-06-04-00	52931	X-ray burst cutoff by ingress.
92040-04-03-00	53569	Data dropout too close to ingress.

Table 3. Orbital Ephemerides of EXO 0748–676

Parameter	Value
T_0 (MJD/TDB)	= 46111.0752010
$P_{\text{orb},0}$ (day)	= 0.15933772840
$n_{b,0}$ (cycle)	= 12526
$T_{b,0}$ (MJD/TDB)	= 48107
$P_{\text{orb},1}$ (day)	= 0.15933782601
$P_{\text{orb},1} - P_{\text{orb},0}$ (ms)	= + 8.43
$n_{b,1}$ (cycle)	= 34515
$T_{b,1}$ (MJD/TDB)	= 51610.7
$P_{\text{orb},2}$ (day)	= 0.15933775443
$P_{\text{orb},2} - P_{\text{orb},1}$ (ms)	= – 6.18
$n_{b,2}$ (cycle)	= 45515.7
$T_{b,2}$ (MJD/TDB)	= 53363.4
$P_{\text{orb},3}$ (day)	= 0.15933783446
$P_{\text{orb},3} - P_{\text{orb},2}$ (ms)	= + 6.91
$P_{\text{orb},3} - P_{\text{orb},0}$ (Net,ms)	= + 9.16

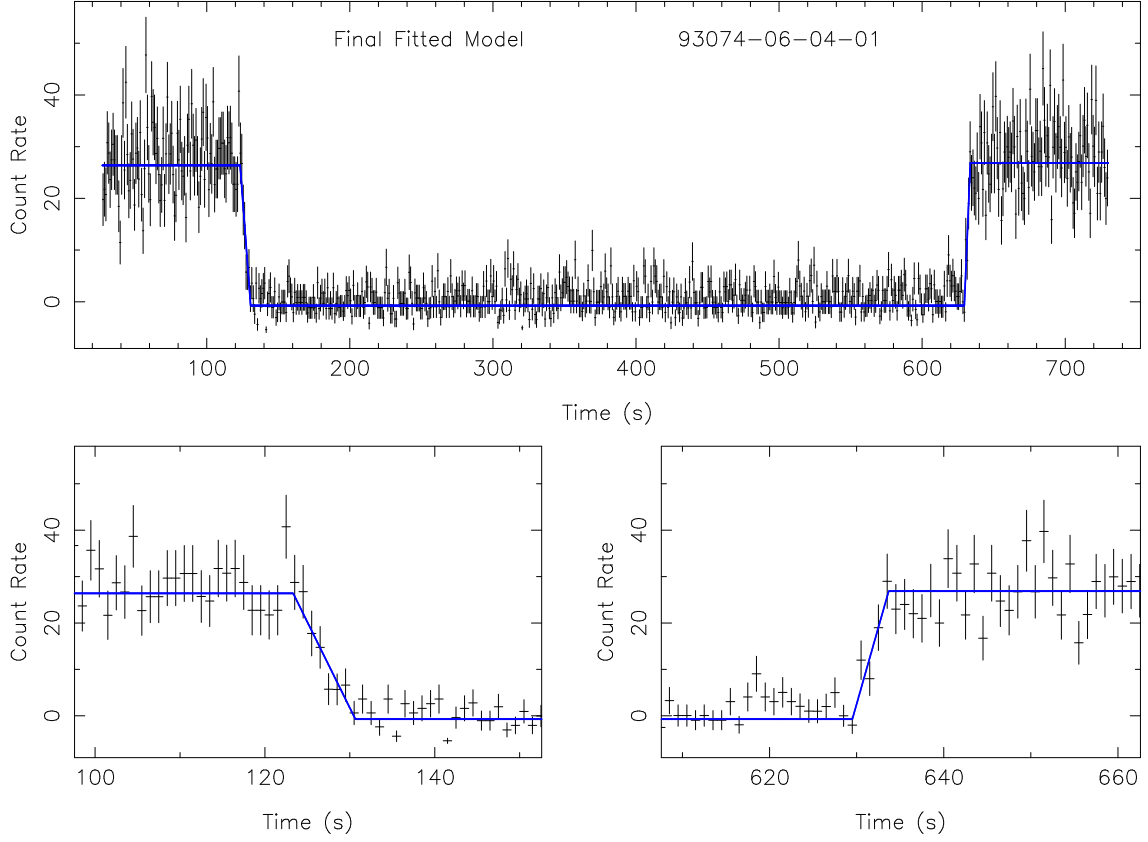


Fig. 1.— A seven-parameter full X-ray eclipse model (blue line) fitted to the X-ray eclipse light curve from the indicated observation. This is a typical fit to one of our eclipse observations. The top panel shows the full light curve and model fit while the two bottom panels show the details of the fits to the ingress (left) and the egress (right) transitions.

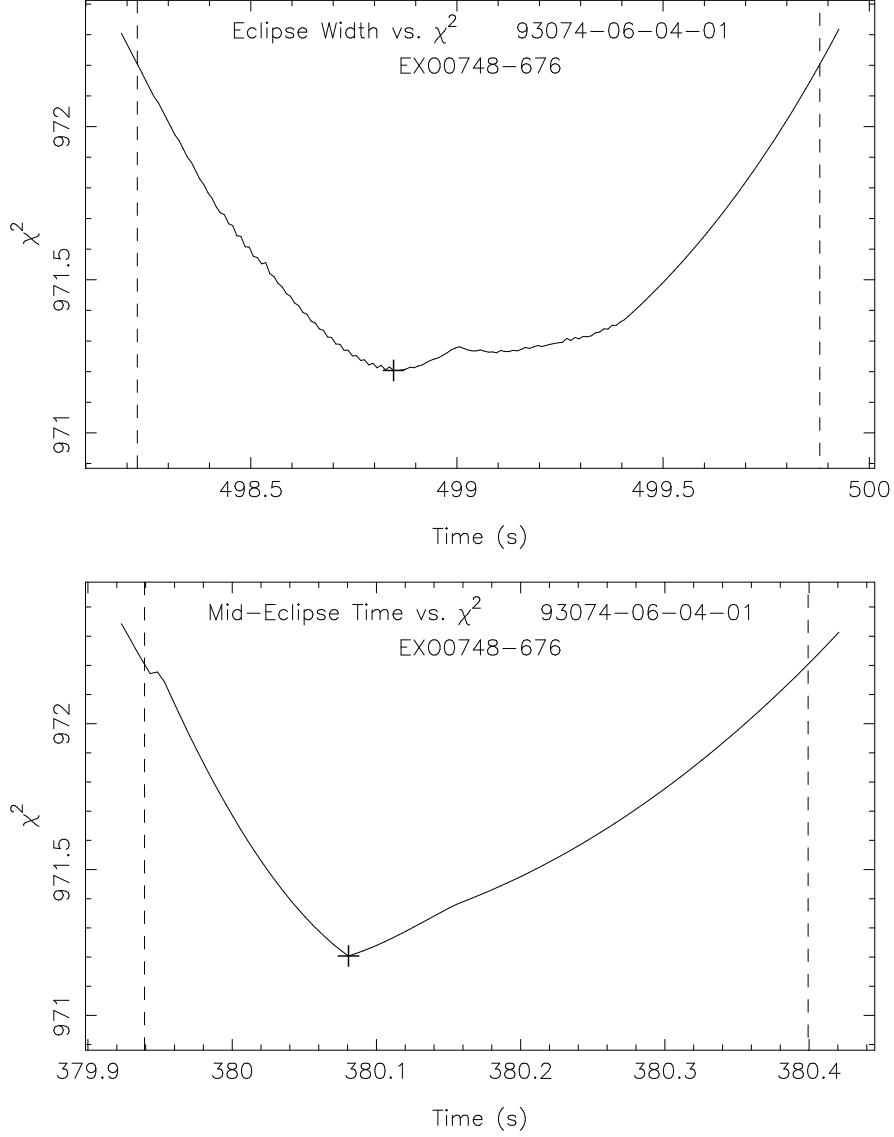


Fig. 2.— χ^2 variation as a function of eclipse width (top panel) and mid-eclipse time (bottom panel) for the fit to the light curve from the observation shown in Figure 1. The bottom panel shows the χ^2 variation with displacement away from the best fit mid-eclipse time and the top panel shows the χ^2 variation with displacement away from the best fit eclipse duration. The best fit value of χ^2 is denoted by the cross on both plots. The dashed lines show where χ^2 crosses a value equal to the minimum value incremented by 1 for both positive and negative parameter variation.

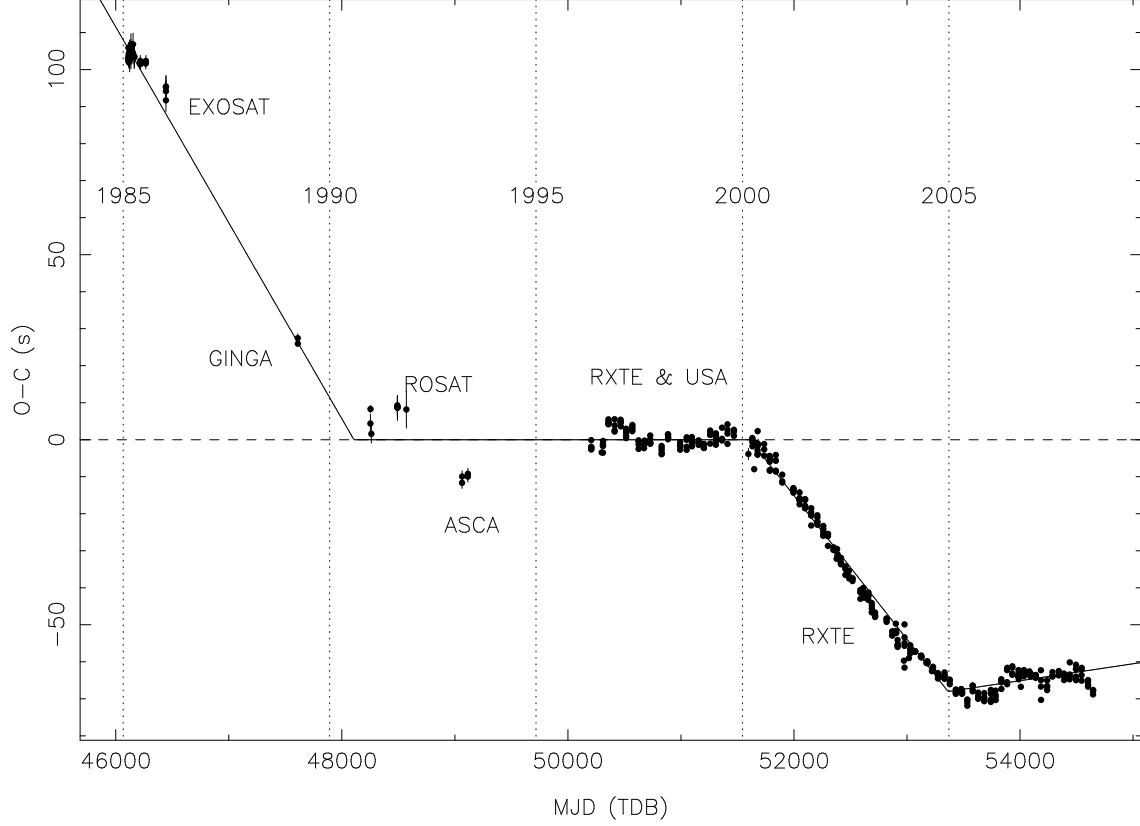


Fig. 3.— The mid-eclipse timing residuals for observed eclipses of EXO 0748–676 during 1985–2008 both from the present study and those available in the literature. The residual of the observed mid-eclipse time is plotted as a function of barycenter corrected observation date. The curved solid line is the four-constant period solution to all the data described in the text. No simple linear or quadratic ephemeris fits all the data points.

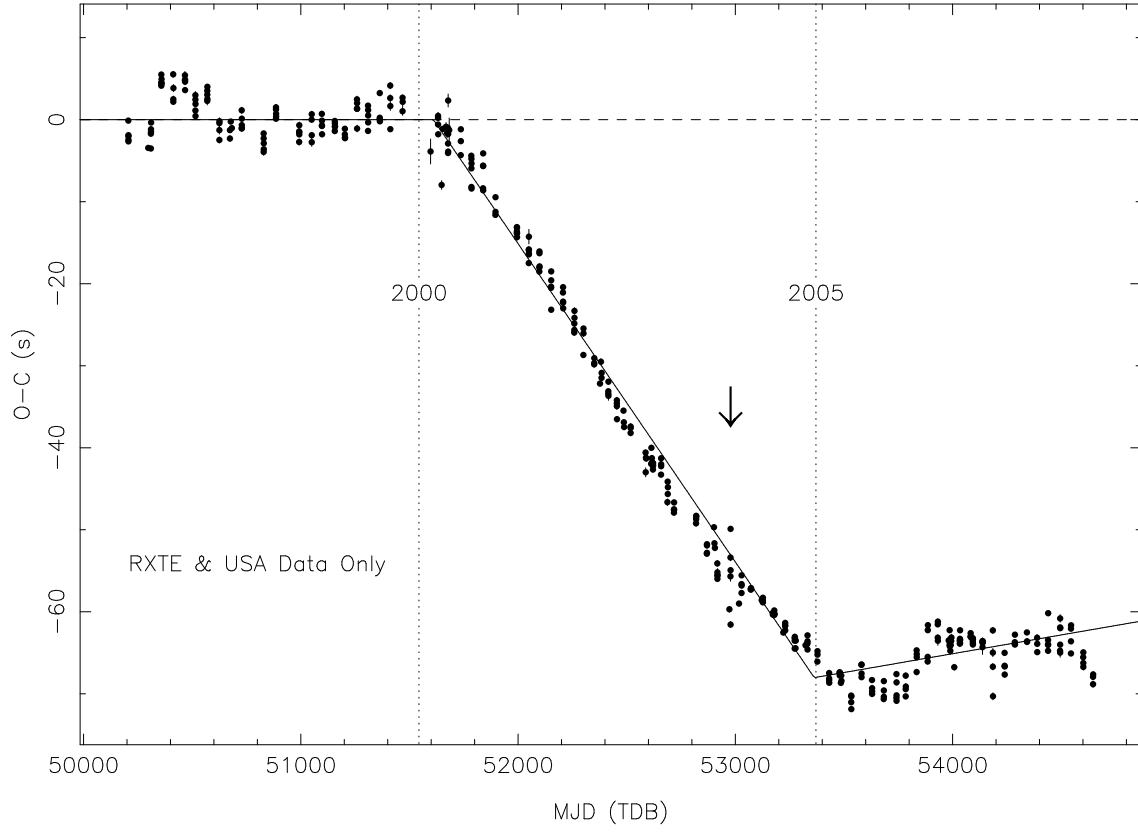


Fig. 4.— The mid-eclipse timing residuals for observed eclipses of EXO 0748–676 during 1996–2008 (the *RXTE* era). The solid line represents the four-constant period solution to all the data. The large variations in $O - C$ values away from the solid line solution at MJD 52978 are the “magnetic loop” eclipses described in Wolff et al. (2007).

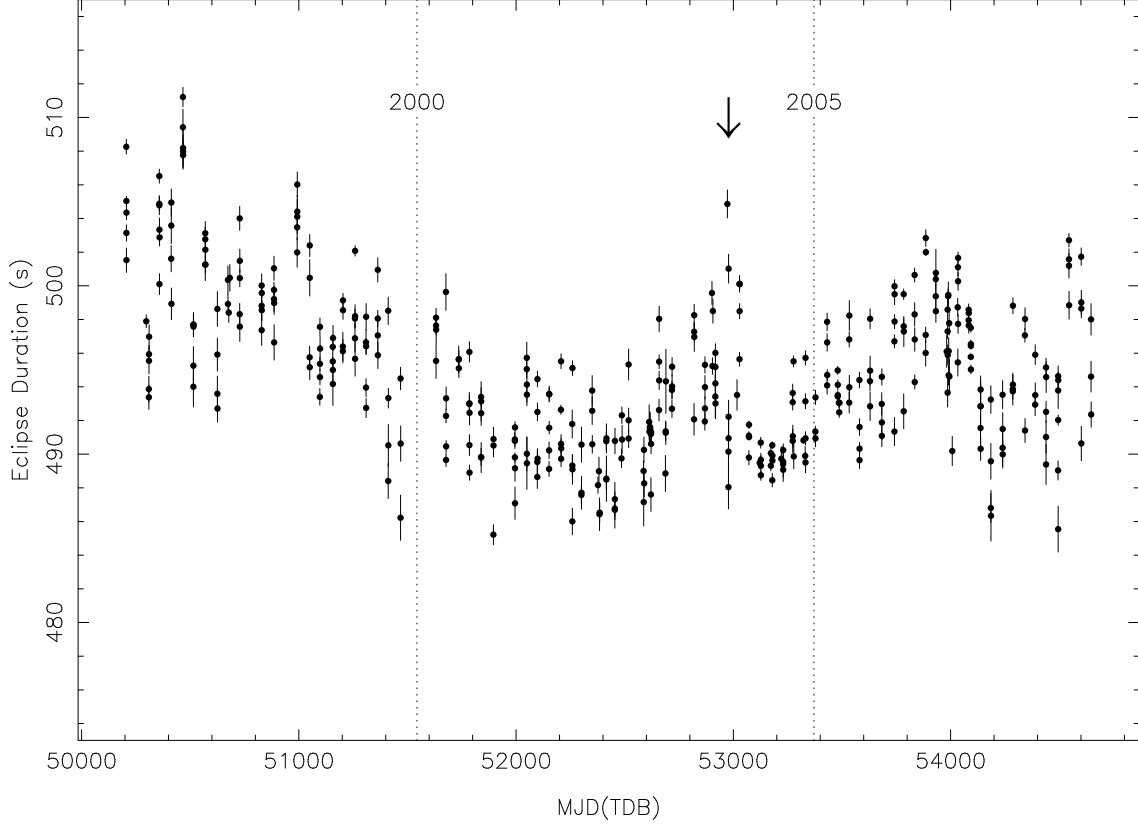


Fig. 5.— The duration of totality (Δt_{ec}) for *RXTE* fitted eclipses of EXO 0748–676 during 1996–2008 from Table 1. Early in the *RXTE* mission eclipse duration appears to shorten as the secondary star undergoes a general contraction. However, near MJD 52000 this trend is reversed as the secondary expands somewhat. The arrow shows the time of the disruptions of the O – C residuals shown in Figure 4. Note also the stable eclipse durations (~ 490 s) around MJD 53200 that have small associated error estimates.